Green Chemistry

ROYAL SOCIETY OF CHEMISTRY

CRITICAL REVIEW

View Article Online
View Journal | View Issue

Cite this: *Green Chem.*, 2022, **24**, 8193

Lignin for energy applications – state of the art, life cycle, technoeconomic analysis and future trends

Anne Beaucamp,[a] Muhammad Muddasar,[a] Ibrahim Saana Amiinu,[b] Marina Moraes Leite,[b] Mario Culebras,[c] Kenneth Latha,[d] María C. Gutiérrez,[e] Daily Rodriguez-Padron,[f] Francisco del Monte,[e] Tadhg Kennedy,[b,g] Kevin M. Ryan,[b,g] Rafael Luque,[f] Maria-Magdalena Titirici[d] and Maurice N. Collins *[a,g]

Received 21st July 2022,
Accepted 5th October 2022

DOI: 10.1039/d2gc02724k

rsc.li/greenchem

Lignin is produced in large quantities as a by-product of the papermaking and biofuel industries. Lignin is the most abundant aromatic biopolymer on the planet with its chemical structure rendering it ideal for carbon materials production and finely tailored architectures of these sustainable carbon materials are beginning to find use in high value energy applications. This review focuses on lignin chemistry, various lignin extraction and fractionation techniques, and their impact on lignin structure/property relationships for energy applications are discussed. Chemistries behind important and emerging energy applications from recent research on this increasingly valuable sustainable polymer are described.

1. Introduction

It is now widely accepted that global warming is a threat to our planet, and it needs to be addressed urgently. To replace petroleum-based products with sustainable materials is a major step in the fight against climate change, as highlighted by the United Nations Sustainable Development Goal (SDG) 9 for Industry, Innovation, and Infrastructure and SDG 12 for Responsible Consumption and production.[1–3] Therefore, the development of sustainable technologies capable of producing new devices using sustainable resources within the circular use of products approach is of critical importance.

Materials used as electrodes greatly influence the performance of supercapacitors, batteries, and thermoelectric materials.[4] Carbon-based materials, such as activated carbon, carbon nanotubes, and graphene nanosheets, have great potential as electrodes owing to their lightweight, high conductivity, and adjustable porosity.[5,6] However, high-quality carbon compounds are usually synthesized using sophisticated and expensive synthesis methods that involve strict chemical conditions, elevated carbonization temperatures, and non-renewable precursors, limiting their extensive commercial use.[7,8] Thus, it is crucial to find easy, efficient, and eco-friendly pathways for producing carbon materials by converting low-cost, sustainable precursors into carbon materials. The utilization of lignocellulosic biomass (cellulose, lignin, hemicellulose) could be a promising alternative route for the synthesis of carbon materials. The scientific community has been attracted to cellulose because of its abundance, adaptability, sustainability, and affordability. The low carbon content in cellulose (44.4 wt%), however, makes cellulose-based carbon materials economically unsuitable for extensive usage.[9] On the other hand, lignin, another biopolymer with high carbon content (≈60 wt%), is the main source of aromatic moieties in the natural world and could be a promising carbon precursor source.[10,11] Lignin is mainly found in plant cell walls, accounting for 20–25% of plant dry weight, making lignin the second most abundant biopolymer after cellulose. However and crucially, the valorisation of lignin is currently limited with 95% of the worldwide lignin being a underutilised by-product of the paper and pulp production and the remainder is used for low value applications.[12,13] The main extraction of lignin is through the Kraft process, which separates efficiently cellulose from biomass. The paper industry burns the black liquor con-

[a]*Stokes Laboratories, School of Engineering, Bernal Institute, University of Limerick, Limerick, Ireland. E-mail: Maurice.collins@ul.ie*
[b]*Department of Chemical Sciences, Bernal Institute, University of Limerick, Limerick, Ireland*
[c]*Institute of Material Science, University of Valencia, Valencia, Spain*
[d]*Department of Chemical Engineering, Imperial College London, London, SW7 2AZ UK*
[e]*Instituto de Ciencia de Materiales de Madrid (ICMM), Consejo Superior de Investigaciones Científicas (CSIC), Calle Sor Juana Inés de la Cruz, 3, Campus de Cantoblanco, 28033 Madrid, Spain*
[f]*Departamento de Química Orgánica, Universidad de Córdoba, Campus de Rabanales, Edificio Marie Curie (C-3), Ctra Nnal IV-A, Km 396, 14014 Cordoba, Spain*
[g]*SFI AMBER Centre, University of Limerick, Ireland*

taining the lignin to generate heat, reused in the production plant through energy cogeneration. The combustion also regenerates the inorganic pulping agent for further use. If the lignin is recovered by acidification of the black liquor, the pulping process produces low-quality lignin, with high sulphur, ash and carbohydrate contents. Therefore, kraft lignin is mainly burnt as a biofuel.[14] Another reason for the poor valorisation of lignin is the complexity and variation of its chemical structure, which is highly dependent on its source and extraction method. Therefore, more profitable value-streams are necessary to motivate a need for a new generation of biorefineries capable of producing high quality lignin fractions. Recent reviews have focused on the refining of lignin,[15] its use for civil engineering,[16] for polymer production,[17] and its use in nanocomposites systems.[18]

This review focuses on the role of lignin in energy applications. The first section briefly describes lignin chemistry and the impact of the extraction method on the quality of the isolated lignin. It also discusses the emerging benefits of fractionation of lignin *via* deep eutectic solvents (DES). Section two details the use of lignin in battery component development with emphasis on anodes, cathodes, binders, electrolytes, separators and redox flow batteries. The following section describes the latest technologies in creating greener and more sustainable supercapacitor electrodes from lignin, starting with simple activation methods and moving towards templated and free-standing carbon electrodes. This leads to a section on an emerging application for lignin in thermoelectric materials where lignin precursor materials are producing nanomaterials with very promising Seebeck coefficients. Section 5 summaries, the production of biofuels from lignin, with particular emphasis on both heterogenous and photo-assisted catalytic conversion of lignin, along with some recent findings on mechanochemical conversion. Finally, we conclude the review with an outlook on the use of lignin in future energy applications.

1.1. Lignin: chemical structure and separation

The word lignin comes from the Latin *lignum*, meaning wood. It is a polyphenolic component of the vascular plant cell wall that cements the cellulose and hemicellulose rods together, creating mechanical support while protecting the plants from microbial attack.[19–21] The amount of lignin depends on the origin of the plant, with softwood (SW) comprising 25–39% of lignin, hardwood (HW) 20–25% and grasses 15–25%.[20] Lignin is the most abundant aromatic biopolymer, with a structure containing over 60% carbon making lignin the source of over 30% of the organic carbon on Earth.[22]

It is biosynthesised by enzymatic dehydrogenation of three monolignols monomers, *p*-coumaryl alcohol, coniferyl alcohol and sinapyl alcohol that differ only by the degree of substitution on the phenolic ring. In the lignin structure, monolignols are present in the form of residue units, respectively *p*-hydroxyphenyl (H), guaiacyl (G) and sinapyl (S). The composition of S, G and H units varies with plant type: SW lignin is mainly composed of S units while HW lignin contains S and G units. Interestingly, grass offers a source of non-methoxylated lignin, containing up to 35% of H units.[23] Within a plant type, proportions of G *vs.* S units would vary depending on the position in the plant and the age of the sample (Fig. 1).[24]

Lignin phenylpropanoid units interlink randomly *via* cross-linking and branching to form an amorphous three-dimensional network.[25] The polymeric structure forms by radical polymerisation, initiated by the action of laccase and peroxidase enzymes.[12,26] Various linkages are formed during the polymerisation, with the most common being ether and carbon–carbon linkages. The carbon in C_β position and the phenoxy oxygen are the most reactive species, making the β-O-4 (β-aryl ether) the most frequent linkage, which can easily be cleaved in an alkaline or acidic medium. The other linkages are more resistant to chemical degradation.[12,24] The formation of chemical bonds during lignification is believed to be mediated by kinetically controlled radical coupling and this has recently been computationally modelled by Gani *et al.*[27] They calculated the value of the activation barrier during radical formation and chain growth of various linkages in G and S rich lignins, with results showing that formation of β-O-4 chains is favourable. Empirically, it was found that the presence of methoxy groups on the 5th aromatic carbon prevents the formation of C–C bonds by β-5 and 5-5 links, rendering branched, condensed lignin rare in its native form.[21,23]

The molecular structure of lignin is dependent on its origin. In particular, hardwood lignins are more rich in phenolic hydroxyl groups (4.3 mmol g^{-1}) displaying a lower molecular weight in comparison with softwood lignins.[28]

To allow separation from the cellulose and hemicellulose rods within wood, native lignin is subjected to chemical processes, which modify the bonding of the polymer by partial depolymerisation – so called technical lignins.[23] The type of technical lignin is as important as the source of lignin. There are three main processes that lead to technical lignins, Kraft, Soda and Organosolv each of which are detailed below.

The kraft process is the largest lignin stream by volume (55 million tons), this high yield process treats wood fibres with a Na_2S/NaOH white liquor at a temperature of 155–175 °C for 1 to 2 hours. Lignin and hemicellulose are dissolved in the solution to form a "black liquor" while the cellulose forms a solid residue. The black liquor, containing 70–80% solid, is usually used as a biofuel in the recovery boiler. This combustion, at 760 °C, produces molten salts of Na_2S and NaOH. These are precipitated and regenerated for circular use within the mill.[36] The kraft lignin can be recovered from the black liquor by precipitation in the presence of acetic acid, which improves the overall mill production.[14] The Kraft process modifies the lignin structure *via* cleavage of the β-ether (C–O) links as well as by demethylation. The formed lignin has a higher degree of condensation through the formation of 5-5 linkages with sulphur added in the form of thiol groups.[23,24] The high ash, sulphur and carbohydrate content of kraft lignin restricts its industrial application to fertilizers, pesticides, binders, aromatic chemicals and resins.[37]

The Soda lignin process is similar to the kraft process, as it uses an alkaline solution (NaOH) at high temperature to separ-

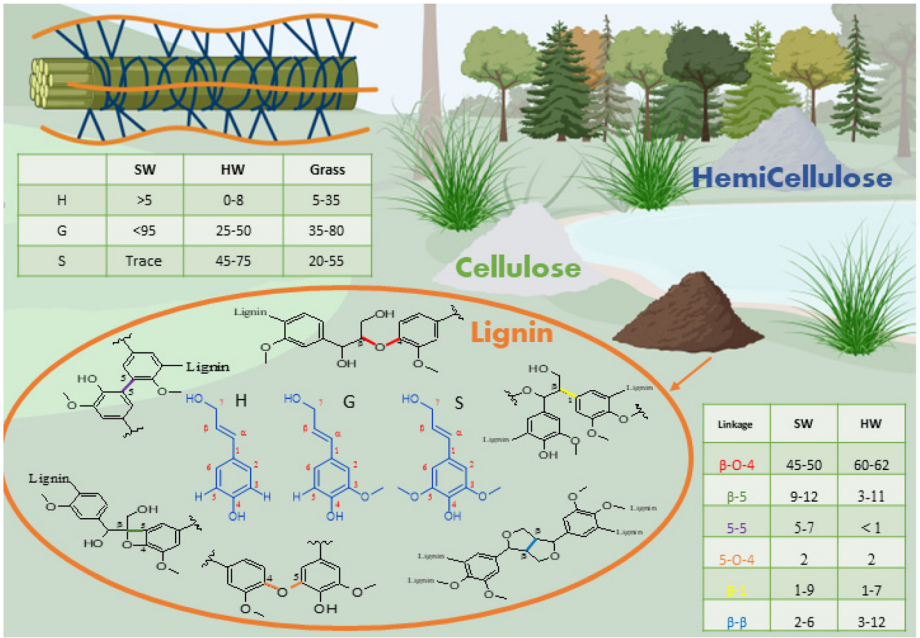

Fig. 1 Structure and chemistry of lignin extracted from plants cell walls.

ate lignin from cellulose by solubilisation. The lignin is then recovered by precipitation at lower pH. This is a sulphur free process, with a yield of 80%, which produces moderately pure lignin, due to the presence of minerals (Na, K) and carbohydrates. The process cleaves the α- and β-aryl ether bonds and produces free phenolic groups but also generates condensation of the aromatic rings.[24,35] The sulphur free soda lignin is used industrially in phenolic resins, animal nutrition, dispersants, and polymer synthesis.

Organosolv lignins are dissolved in organic solvent/water solution at high temperature and pressure. In particular, the Alcell © process uses a mixture of 1 : 1 ethanol : water to dissolve lignin at 180 °C at 13 bars of pressure. The lignin obtained is depolymerised by cleavage of the β-ether links and exhibits a low molecular weight and polydispersity. It also has low ash content and low residual carbohydrate with a general low impurity level.[23,24,35]

Water soluble lignosulfonate or sulphite lignin is formed by reaction between lignin and metal sulphite salts. The reaction can be processed at pH varying between 2 and 12. This process cleaves α and β-ethers and forms a high quantity of sulfonic acid groups on the C_α position.[38] Lignosulfonate has the highest molecular weight (up to 50 000 g mol^{-1}) due to condensation between the aromatic rings. Sulphite lignin is mostly used as an additive in the construction industry thanks to its solubility in water.[37]

Other methods such as Milled Wood Lignin (MWL) or enzymatic lignin produce low sulphur content lignin. MWL is obtained by washing finely milled biomass by a neutral solvent such as dioxane/water. The solution is then centrifuged, the solid freeze-dried and washed.[39,40] This process extracts lignin that is essentially structurally unchanged from the biomass it originates. This method has a low yield and is usually carried out for native lignin characterisation studies.[39,41,42] Steam explosion lignin is produced by rapidly decompressing a high-pressure biomass-steam mixture to separate the biomass. The liquid recovered is washed at low pH and the lignin is isolated. This method produces high quality sulphur-free lignin, with minor structural modifications and at a low cost.[43] Enzymatic hydrolysis involves the hydrolysis and dissolution of carbohydrates by cellulase enzyme. This process aims to produce bioethanol and the lignin is recovered as a by-product, with moderate amount of impurities.[44]

The water solubility of lignin is displayed in Table 1. Most lignins are soluble in alkaline conditions due to the presence of phenolic groups, whose amount can be increased depending on extraction conditions. While lignosulfonates are fully soluble in water due to their extraction conditions.

Current research uses all lignin streams for the development of high-end applications such as nanostructured materials, fine chemicals, carbon materials and biofuels. Kraft lignin and organosolv lignin are the preferred materials due to the availability of Kraft and the high purity of organosolv. While lignin is heterogeneous in terms of secondary groups, the main characteristic of the macromolecule are its phenolic groups that allow for reactivity, solubility and modification. The thiolation observed on Kraft lignin can be reversed by thermal treatment: the thermal decomposition of sulphur containing lignin releases sulphur dioxide (SO_2) and methylated sulphur compounds as the thiol groups are breaking down. Dondi *et al.* measured the amount of sulphur compounds released during pyrolysis. The release of SO_2 was maximum at 253 °C while CH_3SH and CH_3SCH_3 were released at 266 °C. The authors also investigated the release of CO_2, and it was

Table 1 Production volume, yield, chemical composition and water solubility of various technical lignins. Data from ref. 24 and 29–35

	Production volume (tonnes per year)	Yield (%)	Impurities (%)	Molecular weight (Mw) and polydispersity	Solubility in water
Kraft lignin	55 000 000	90–95	Sulphur: 1–3 Ash: 0.5–3.0 Carbohydrates: 1.0–2.3	1500–5000 (2.5–3.5)	Fully soluble in pH > 12
Lignosulfonate	1 000 000	70–95%	Sulphur 3.0–8.0 Ash: 4.2–7.0 Carbohydrates: N/A	1000–50 000 (6.0–8.0)	Fully soluble
Soda lignin	6000	>80	Sulphur: 0 Ash: 0.7–3.0 Carbohydrates: 1.5–3.0	1000–10 000 (2.5–3.5)	Fully soluble in pH > 12
Organosolv	1000 (pilot Scale)	25–50	Sulphur: 0 Ash: 1.7 Carbohydrates: 1.0–3.00	500–5000 (1.5–4.4)	Fully soluble in pH > 12
Milled Wood Lignin (MWL)	Lab scale	20	Sulphur: 0 Ash: 1.5 Carbohydrates: 0.30	5500–20 000 (1.8–2.5)	Poor
Steam Explosion Lignin (SEL)	Lab scale	>90	Sulphur: 0–0.5 Ash: 5.0–8.0 Carbohydrates: 2.5–4.0	1000–15 000 (2.5–7.0)	Fully soluble in pH > 12
Enzymatic lignin/ hydrolysis lignin	Lab scale	95	Sulphur: 0–1 Ash: 1.0–3.0 Carbohydrates: 2.5–4.0	2000–4500 (1.5–3.2)	Fully soluble in pH > 12

found to be one order of magnitude higher for Kraft lignin. It was hypothesised that this increase is due to the oxidative nature of the sulphur compounds.[45] A similar study from Han[46] showed that below 250 °C, SO_2 is the only compound released during fast pyrolysis.

1.2. Deep eutectic solvents and aqueous dilutions thereof for lignin fractionation

Valorisation of lignocellulosic biomass into high-value-added products including biofuels, bio-based chemicals and biomaterials relies on the development of suitable biorefineries. The lignocellulosic-based biorefineries suffer major bottlenecks, such as the design of pre-treatment techniques.[47] For pre-treatment the most important requirements include (1) sustainability (with cost-effective and environmentally friendly solvents/reagents), (2) universality (suitable for a wide range of lignocellulosic biomass materials) and (3) delignification efficiency (capable to provide the individual constituents of lignocellulosic biomass with high yield and purity whilst allowing their conversion into value-added biochemicals).

In this context, Deep eutectic solvents (DESs) have attracted much attention for lignocellulosic pretreatment.[48–51] DESs are formed by hydrogen bond (HB) complexation between (at least) two molecules, one hydrogen-bond donor (HBD) and one hydrogen-bond acceptor (HBA). Examples of HBAs typically used for DESs formation include many different ammonium and phosphonium salts while alcohols, acids, amides, *etc*. are representative of HBDs.[52] The most often cited rationalisation for this phenomenon is that the charge delocalisation occurring through HB between halide anions with hydrogen-donor moieties is responsible for the decrease in the freezing point of the mixture relative to the melting points of the individual components. Recent *ab initio* molecular dynamic simulations[53] and neutron diffraction studies[54] have revealed the occurrence of many possible HB interactions of different strengths among DES constituents, forming an extended HB network similar to those found in crystalline structures. In this regard, inelastic neutron scattering studies have indicated that eutectic behaviour emerges when the components mix *via* HBs, the strength of which is weak enough to prevent them from settling into a co-crystal.[55] Moreover, ternary or quaternary DESs can be formed by combination of more than one HBA and/or more than one HBD.[56,57]

DESs are particularly well-suited to fulfil most of the above-mentioned requirements as they exhibit remarkable green features (*i.e.*, main DESs components are non-toxic, highly biodegradable and biocompatible), they succeed in the treatment of a large number of lignocellulosic biomass materials (*e.g.*, douglas fir, poplar, sorghum, corncob, walnut endocarps cells, peach endocarp cells, wheat straw, corn straw, rice straw, castor seed coat, oil palm empty fruit, bunch, willow, switchgrass, *Eucalyptus camaldulensis*, *Eucalyptus globulus*,

Cunninghamia lanceolate, *Cortex albiziae*, *Arabidopsis thaliana* and *Pinus pinaster Ait*, among the most relevant) and they provided delignification efficiencies of up to 95% with purities of the obtained lignin in the range of 76–98% with certain abundance of β-O-4 linkages, the presence of which is critical for the subsequent valorisation of lignin (*e.g.*, β-O-4 linkages determine the high-yield production of aromatic monomers). Moreover, DES can be recovered after lignin fractionation and reused in subsequent pre-treatment processes (Fig. 2).[58] For further details on this topic can be found in some excellent reviews recently published.[48–51]

Nonetheless, it is worth noting that while the fulfilment of requirements (1) and (2) by DESs is remarkable, work must yet be done to obtain well balance results in (3). For instance, lower temperature, shorted time, or higher solid loading give rise to a higher percentage of preserved β-O-4 bonds in DES lignin.[59] Moreover, DES constituents, both the HBA and the HBD, also play a role in lignin fractionation performance. For instance, it has been demonstrated that the relevance of the nature and number of functional groups of the HBD id of importance. Thus, most effective HBDs for lignin fractionation are monocarboxylic acids. In this sort of acid-based DESs, the stronger and the higher the molar ratio of the acid, the higher the fractionation yield (*e.g.*, up to 93.1% for a DES composed of lactic acid, LA, and choline chloride, ChCl, mixed in a LA : ChCl molar ratio of 15 : 1).[60] Hydroxyl groups in HBDs have proved less effective than carboxylic acids for lignin fractionation.[61] In either case, the increase of the number of functional groups exerted a detrimental effect on delignification. It seems that the eventual HBA participation in a more extended HB network weakens its ability to compete with intra-molecular bonding in the lignin moieties of biomass.[62] Particularly interesting among this hydroxyl-based DESs are those formed with phenolic compounds given their capability to form new strong π–π stacking interactions and HBs with lignin moieties.[63] It is also worth noting that the ability of DESs with amine/amide-based for lignin fractionation. In this case, it is hypothesized that the presence of amine/amide groups in HBDs endows the DES with strong basicity that facilitates lignin fractionation by loosening various chemical bonds of LCC and contributes to selective dissolution through the deprotonation of phenolic moieties in lignin. Finally, although less studied, HBAs can also play a significant role in the performance of lignin fractionation by the contribution of the halide anions to the breakage of β-O-4′ bonds thus preventing lignin condensation.[64]

However, it is worth noting that, as mentioned above, stabilisation of β-O-4 linkages are critical for the subsequent valorisation of lignin and this stabilization generally occurs at the expense of lignin fractionation yield and purity. Thus, the challenge for DES-based lignocellulosic pretreatments is the achievement of not only high lignin fractionation yield and purity but also with good preservation of β-O-4 linkages. In this regard, this review focuses on recent and promising research emphasising what we believe should be the future directions to explore. Among others, we think, most intriguing attempts are lately involving the use of aqueous dilutions of DESs.[65–68] The nature of aqueous dilutions of DESs (*e.g.*, reline, a DES formed by complexation between choline chloride and urea mixed in a 1 : 2 molar ratio) was first studied in detail in 2009.[69] That work described how, in a highly diluted regime, the original HB complexes of DES were broken and, as most of the DES components are soluble in water, the system became a simple aqueous solution of the individual DES components. Interestingly, the scenario in a less diluted regime is quite the opposite with the HB complexes of DES solvating H_2O molecules. Actually, neutron scattering measurements have revealed how H_2O molecules are interstitially accommodated within the DES-based HB network.[70] This accommodation not only happens for H_2O but also for other solvents with HB capabilities (*e.g.*, methanol, benzyl alcohol, DMSO, *etc.*) as indicated the deviation from ideality observed in excess properties such as molar volume (V^E), viscosity (η^E) or compressibility ($\Delta\beta_S$).[71–74] Interestingly, all these liquid binary mix-

Fig. 2 Schematic representation of the DESs pre-treatment process. Reprinted with permission from ref. 58. Copyright 2022, Elsevier.

tures exhibited viscosities that are below that of the original DES, which is indeed of relevance for practical applications.

This reduction in viscosity is obviously of help for the effectiveness of aqueous dilutions of DESs no matter the mechanism (*e.g.*, hydrotropic or co-solvency, Fig. 2) behind lignin solubilisation. The hydrotropic mechanism is particularly effective for DESs composed of HBDs and HBAs capable to act as hydrotropes.[75] More intriguing is the co-solvency mechanism.[76] DESs following the co-solvency mechanism are all formed by water-soluble and/or water-miscible compounds (*e.g.*, ethylene glycol, formic acid, propionic acid, lactic acid as HBDs and tetrapropylammonium chloride and choline chloride as HBAs). In these cases, the amount of H_2O is by no means trivial, changing its role from co-solvent to anti-solvent when it surpasses a certain content. Whether there is a correlation between amount of H_2O providing the best results of lignin dissolution and that in which DES aqueous solutions exhibit the largest deviations from ideality may bring some light to better understand the rationale behind lignin solubilisation in DES aqueous solutions.

Moreover, this co-solvency mechanism for lignin dissolution resembles that described for the lyocell process, in which *N*-methylmorpholine-*N*-oxide (NMMO) in its monohydrate form is used for cellulose dissolution. It is widely accepted that NMMO dissolve cellulose by their capability to form HBs (*e.g.*, NMMO-cellulose-HBs) with cellulosic units, replaces the intermolecular and intramolecular HBs between D-glucose units and thus breaks the complex HB network of cellulose.[77,78] H_2O is a serious competitor for NMMO to form HBs with cellulose (*e.g.*, H_2O-cellulose-HBs). Thus, the $1NMMO:1H_2O$ mixture works well because there are still sufficient NMMO-cellulose-HBs (more so than H_2O-cellulose-HBs) and the viscosity of the solution is lower than without H_2O. Recent works have demonstrated how the addition of co-solvents with HB capabilities can help cellulose dissolution by further decreasing the viscosity while preserving the favoured balance between NMMO-cellulose-HBs and H_2O-cellulose-HBs.[79,80] Based on this, the use of environmentally friendly co-solvents with HB capabilities that can replace H_2O totally or partially which may offer interesting sustainable perspectives for future processes in the valorisation of lignin for high value energy applications.

2. Lignin for energy applications – batteries

Lignin has been identified as an excellent precursor for the synthesis of various active carbon-based materials for energy storage devices. However, to date, their inherently poor electrical conductivity has largely hindered their direct use as electrode materials in energy storage and conversion devices. Therefore, various synthetic methods and structural transformation strategies have been pursued to enhance their conductivity, electrochemical and thermomechanical properties. The most common strategy for converting lignin to battery active carbon materials is by pyrolysis at high temperatures (600–1100 °C) using chemical activation agents (*e.g.*, KOH, K_2CO_3 and $ZnCO_3$).[81–83] The combination of these synthesis steps effectively converts the large polyaromatic macromolecules of lignin into an active carbon that is suitable for battery applications. This introduces several key features that bequeath the carbon derivative with advanced properties such as a hierarchical nano-micro pore system (Fig. 3a), high conductivity and mechanical robustness which benefit fast kinetics, high stability and high charge storage capacity. Like graphite, lignin derived carbons have been widely explored in various energy storage applications, including metal ion (Li^+, Na^+, K^+, *etc.*), metal oxygen and redox flow batteries.[81] However, unlike graphite, the polymeric nature of lignin allows for functionally tailored modifications, including surface functionalisation and molecular grafting prior to carbonisation and heteroatom doping, leading to carbon materials with various morphologies and enhanced functional properties. This enables lignin-derivatives to exhibit beneficial properties spanning the whole chain of the battery component development (*i.e.*, anode, cathode, binder, separator and electrolyte). Therefore, the high structural flexibility of lignin to exhibit various functions makes it a highly attractive precursor material for carbon-based battery materials.

2.1. Lignin derived anode materials

2.1.1. Li-ion batteries anodes. Here, the potential of lignin derived anode materials for Li-ion batteries (LIB) is highlighted and contrasted with that of graphite, the conventional anode material deployed in commercial LIBs. Graphite possesses good electrochemical properties as an anode material such as long cycle life, low average voltage without inducing Li plating, as well as low irreversible capacity, small volumetric change during lithiation, high coulombic efficiency (CE), good thermal stability, good electronic conductivity and high structural stability. However, the major disadvantage of pure graphite-based Li-ion anodes is that they have reached their theoretical limit in terms of their practical specific capacity, making it highly critical now to develop higher capacity electrode materials to further boost energy density. Furthermore, natural graphite is a limited resource and is on the US and EU's list of critical raw materials. While synthetic graphite can be produced readily, it is more expensive than natural graphite and its synthesis is energy intensive and requires unsustainable precursors from the fossil fuel industry.[84] As such, more sustainable carbon-based Li-ion anode materials with higher energy densities are urgently required.

Carbon based materials of various morphologies and structures have been widely used as anode materials in different battery chemistries and have been modulated to meet different requirements. Porous and fibrous carbons are the most researched electrode materials and are typically obtained from organic chemical compounds with high cost and negative environmental impacts. Lignin on the other hand is eco-friendly and a naturally abundant precursor for low-cost production of hierarchically porous carbon and nano fibre-based

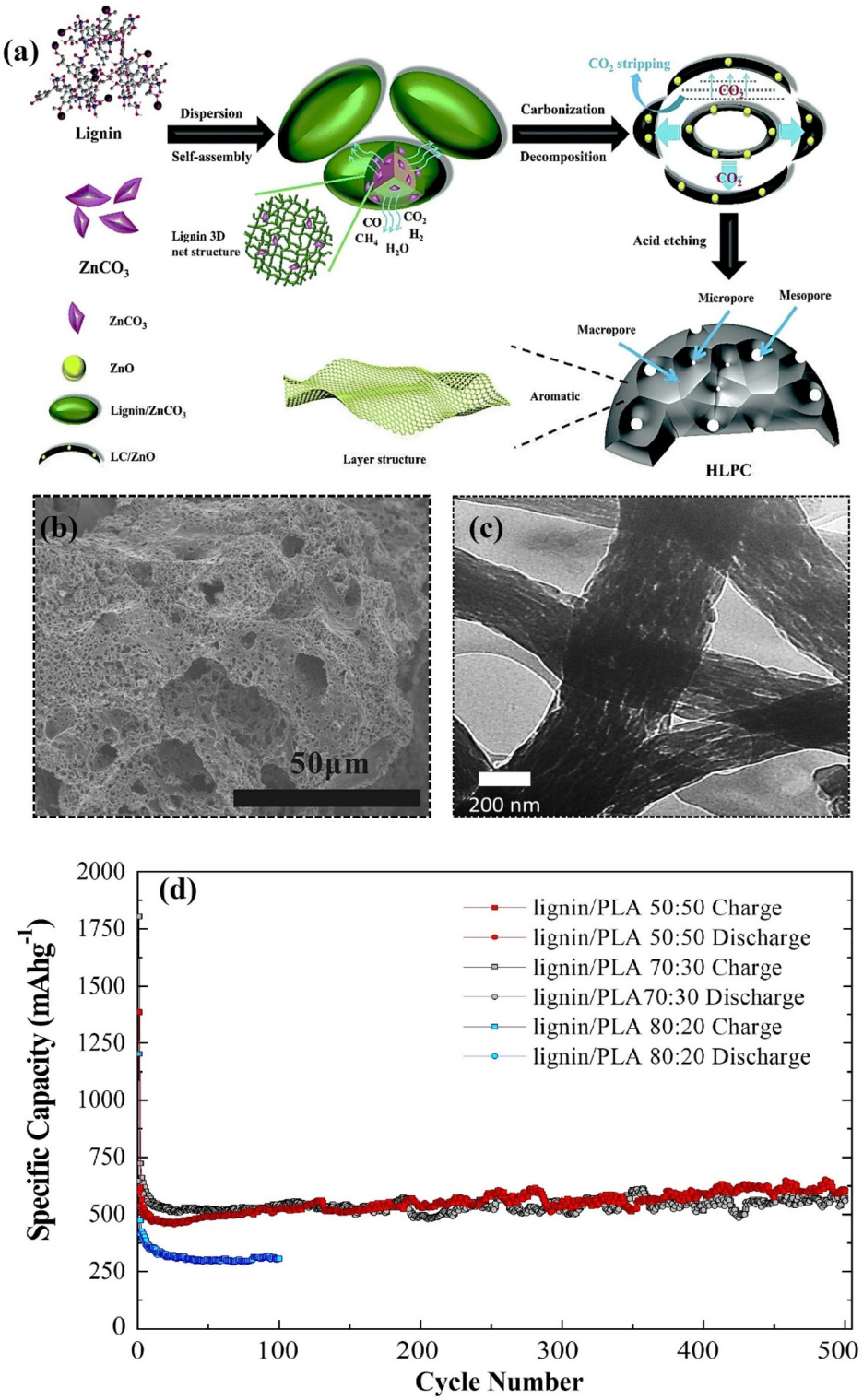

Fig. 3 (a) Synthesis route to hierarchical porous carbon anode from lignin. Adapted with permission from ref. 96. Copyright 2020, Royal Society of Chemistry (b) SEM image showing hierarchical porosity of lignin-derived carbon anode. Adapted with permission from ref. 85. Copyright 2015, Elsevier (c) TEM image showing hierarchical porosity of lignin-derived carbon nano fibre anode. (d) Anode cycling performance of lignin/PLA derived CNFs at C/2. Adapted with permission from ref. 86. Copyright 2019, Wiley-VCH.

electrode materials. The porosity enhances the surface area for rapid mass transport of ionic species. For example, Lu's group[85] developed a hierarchical porous carbon *via* the pyrolysis of a lignin/KOH mixture at 700 °C for use as an anode in LIBs (Fig. 3b). The introduction of 3D network of pores within the carbon framework enhances the surface area (907 $m^2\ g^{-1}$) for efficient diffusion of ions, leading to a better charge storage capacity (386 mA h g^{-1}) at 200 mA g^{-1} after 560 cycles compared to the carbon without pores (77.1 $m^2\ g^{-1}$, 124 mA h g^{-1}). The significance of pore structures, high surface area and networking was demonstrated by Culebras *et al.*[86] in which a homogenized blend of lignin and polylactic acid (PLA) was electrospun and subsequently carbonized at 900 °C into fine porous carbon nano fibres (CNFs) (Fig. 3c). The lignin/PLA (50 : 50%) based CNFs exhibited a surface area of 670 $m^2\ g^{-1}$ which enhances the ion transport and cycling stability as a LIB anode, delivering a capacity of 611 mA h g^{-1} after 500 cycles (Fig. 3d), which is almost twice the theoretical capacity of graphite (372 mA h g^{-1}). While the capacity of lignin derived carbons is higher than graphite, they still exhibit low initial coulombic efficiency (CE) and the use of organic polymer blends and chemical activation agents at high temperatures tend to weaken the environmental benefits. Moreover, the demand for high energy density batteries particularly for electric mobility applications cannot be satisfied with only lignin derived carbon materials. However, the capacity of carbon anodes can be improved by incorporating high capacity materials such as Si (theoretical capacity: 3579 mA h g^{-1}) into the carbonized lignin matrix.[87–89] It is important to note that while Si exhibits high capacity characteristics, the application of anodes based solely on bulk Si or micron sized particles is limited by the huge volumetric change (>300%) during cycling which can lead to pulverisation of the material and delamination from the current collector with irreversible capacity losses.[90–95] Therefore, composite anodes of Si/carbon are critical for the next generation of high performance LIBs as the stability and energy density can be significantly boosted.

Such composite electrode concepts have been demonstrated by Niu and coworkers[87] where the lignin-derived carbon networks cross-linked the Si nanoparticles and delivered a stable capacity of ~2670 mA h g^{-1} at 300 mA g^{-1} after 100 cycles with the CE increasing from 62 to >99%. Although the capacity is largely owed to the Si, the lignin derivative played the key role of enhancing mechanical stability, boosting the conductivity while also contributing to the capacity. While lignin anodes exhibit high promise as next-generation electrodes to replace graphite in LIBs, the study is largely limited to half-cells. To advance the development of lignin-based anodes in practical batteries, their characterisation and detailed analysis in full cell configurations should be explored. In a full cell, the actual working voltage range of the anodes can be reduced, which may lead to a decrease in capacity especially when the voltage profile has a sloping region. This will affect the overall battery energy density, but it is hard to distinguish the contribution of each electrode since the signal is a contribution of both cathode and anode. Such studies are lacking to date. This is particularly crucial for composites anodes such as Si/lignin electrodes which hold high promise as high energy density battery components for electric vehicle and robotic applications.

For lignin-derived anodes, in most cases thy display electrochemical cycling stability for over 100 cycles, it is essential to investigate the contributing factors and the mechanism inducing the longer cycling capacity decay that is unique to lignin. It is also essential to investigate the influence of safety issues such as rate of formation and potential impact of delamination effects, and the mechanical and thermal tolerance characteristics on the long-term battery performance and stability.

2.1.2. Negative electrodes in Na^+ and K^+ batteries. It has been over three decades since LIBs were first introduced in the market. Owing to their high energy density, they have become ubiquitous for mobile applications. With the increasing demand for LIBs, concerns have been raised about the scarcity of the necessary resources, pointing to the need to diversify battery chemistries. With that in mind, Na-ion batteries (SIB) have come back to the spotlight, joined by K-ion batteries (KIB), especially for stationary applications. In comparison to LIBs, SIBs and KIBs rely on more abundant and widespread elements (Na and K, for example), more sustainable precursors and materials, leading to lower cost and potentially safer technologies.[97–99] Despite their similar chemistries, there are significant differences between them and many challenges to be overcome to commercialize SIBs and KIBs. Although graphite is the state-of-the-art negative material in LIBs, it is not suitable for Na^+ intercalation. The low thermodynamic stability of Na-graphite intercalation compounds leads to low capacities[100] unless co-intercalation phenomena occurs *via* combination with ether-based electrolytes.[101–105] On the other hand, hard carbons (HC) are electrochemically active in standard carbonate-based electrolytes[106] as their disordered structure promotes wider interlayer spaces between the graphene sheets which allows for reversible intercalation of Na^+. Furthermore, Na^+ can be accommodated in micropores present in hard carbon which adds to the gravimetric capacity of the anode.[107] Hard carbons can be obtained from biomass, especially from lignin with its high carbon content. Moreover, the aromatic backbone of lignin can provide structural rigidity and lead to more thermally stable materials.[108] The precise Na^+ storage mechanism in hard carbons is still under debate, but it is broadly known that it consists of three main processes: intercalation between graphene layers; adsorption on layer surfaces; and pore filling.[109] The combination of these processes leads to typical galvanostatic charge/discharge profiles with a sloping region between 1.0 and 0.12 V and a plateau region below 0.12 V *vs.* Na/Na^+. The presence of terminal H bonded to the carbon backbone, heteroatoms such as O and N and defects can affect the curvature of the graphene layers, widening the interlayer *d*-spacing and enabling the intercalation of Na^+ ions. Simultaneously, defects act as sites for the adsorption, enhancing the Na^+ storage capacity of hard carbon.[110] The wide variety of storage processes means the performance of lignin-derived hard carbons is dependent on a range of properties which include the material's crystalline composition, graphene

interlayer spacing, porosity, particle morphology and surface composition. This section aims to show some of the effort towards the tuning of those properties in producing lignin-derived HC.

Dou *et al.* compared the performance of HC derived from pectin, hemicellulose and lignin in Na-ion batteries.[111] The lignin-derived material presented the highest capacity (298 mA h g^{-1} at 20 mA g^{-1}) and highest initial coulombic efficiency (68%) among the three. Despite having the lowest BET surface area (only 30 cm^2 g^{-1}, in comparison to 223 cm^2 g^{-1} for the hemicellulose-derived HC), their lignin-derived hard carbon showed higher mesoporosity. The pore size, combined with the presence of graphitic carbon and the higher purity of the material explain its better performance. A low-temperature pre-oxidation step was found to have an important effect on the produced HC performance by increasing the interlayer distance of the carbon sheets[112] and stabilizing the structure to prevent it from rearranging the graphene layers during the high-temperature carbonisation.[113] Using a phenolic resin precursor, the pre-oxidation step promoted better cycling stability, but did not improve the capacity of the materials significantly.[114] Ghimbeu *et al.* noticed an abrupt capacity fade after 30 cycles in a lignin–sulfonate-derived HC, caused by the presence of impurities (mainly Na, K and S from the lignin extraction process).[115] Including an aqueous washing step in their synthesis promoted a higher capacity and better cycle stability. Other works include washing steps with acids to remove the impurities from lignin precursors.[111,116–119] Peuvot *et al.* tested different temperatures to carbonize stabilized lignin fibres.[120] fibre diameter, surface area and the cycling performance of the produced materials varied depending on the carbonisation temperature (from 800 °C and 1700 °C), with 1200 °C found to be the optimum temperature in their study. Many works investigate the effect of carbonisation temperature, with the best results between 1200 °C and 1400 °C (see Table 2).[121] Doping HC with anions can improve their performance, inducing the presence of defects and increasing the number of active sites. Several methods can be used to dope HC from lignin. For instance, Fan *et al.*,[122,123] used a hydrothermal method to produce a mixture of lignin and 3-aminophenol. After carbonisation, the N-doped carbons presented more defects, larger interlayer *d*-spacing, lower charge transfer resistance and higher porosity, leading to a 2.7-time increase in capacity at 50 mA g^{-1} (115 mA h g^{-1} to 315 mA h g^{-1}).[122] The adsorption of Na^+ on defects can take place at a wide range of potentials, thus contributing to the capacity at the sloping region. In this case, the sloping region capacity increased from 62 mA h g^{-1} (non-doped material) to 104 mA h g^{-1} (N-doped material) at 100 mA g^{-1}. In this case, high reversibility was achieved, however it should be noted if the binding energy of Na^+ to the defects is too high, as in the case of B doping,[124] adsorption is not reversible. Other sources of N can be used, such as melamine and urea.[125] The methods and modifications that can be applied to lignin precursors are countless and much research is still necessary to reach a full understanding of their impact on the performance of the produced carbons.

Biomass-derived hard carbons have also been applied as potassium-ion battery (KIB) anodes.[126–132] The K^+ storage mechanism is based on adsorption of ions onto the surface of graphene sheets and the intercalation of ions in graphitic regions[133] similar to the Na-ion case. In KIBs, the mechanism originates a galvanostatic charge/discharge profile characterized by two different regions: a high-inclination slope at higher potentials (from 1.2 to 0.4 V *vs.* K/K^+) and a low-inclination slope below <0.4 V. Despite the low first cycle coulombic efficiency (<50%), recent progress led to lignin-derived HC with capacities as high as 355 mA h g^{-1} at low current rates.[131] Wu *et al.* compared lignin with different molecular weights, reaching 300 mA h g^{-1} at 50 mA g^{-1} for their medium weight precursor (9660 g mol^{-1}). Liu *et al.*[132] produced a HC from maple leaves and further treated it with concentrated HNO_3 for chemical activation and doping with N and O. Their product exhibited good cyclability, with a capacity of 141.9 mA h g^{-1} at 1 A g^{-1} in the 1000th cycle. The development of similar hard carbons from lignin and other bio sources could be a key to boost K-ion technology to a competitive standard.

Despite the numerous examples of high capacity and good cyclability of carbons from lignin as anodes in metal-ion batteries, proper control of carbon structure and porosity is still a challenge. Different bio sources can be used to obtain lignin as a hard carbon precursor.[134] The characteristics of the precursor lignin depend both on its source and on the separation/extraction process. Composition, amount of impurities, molecular weight, polydispersity and solubility are some of the characteristics that can change drastically with the extraction method.[135] On their turn, they will affect the carbons' morphology, porous structure, surface composition and hence the final performance in a battery. Unfortunately, a thorough characterization of the precursor lignin is not always shown in the literature, making it hard to draw trends correlating lignin features with the derived carbon properties. Adding to the heterogeneity of lignin precursors is the variety of possible modification steps and the carbonization process itself, rendering a multitude of variables to be considered in the transformation of lignin into metal-ion battery anodes. Working with so many variables, although a challenge, is also encouraging due the great potential to achieve better materials.

SIBs, similar to LIBs, can also work with alloying anodes, where a reversible reaction takes place by alloying and de-alloying Na in the negative electrode instead of adsorption and intercalation of Na^+. Despite the high capacities delivered by alloying, it is accompanied by drastic volume changes that can degrade the electrode in just a few cycles. To achieve good cyclability with a Sn anode (91% of capacity retention after 1000 cycles) Wang *et al.* employed lignin as a precursor to form Sn/C particles.[136] Similar approaches could be investigated to enable different alloying metal anodes for high energy density SIBs and KIBs in the future.

2.2. Lignin derived cathode materials

2.2.1. Li–S batteries cathodes. Li–S batteries (LSBs) are notable for their much higher specific energy (450 W h kg^{-1})

Table 2 Hard carbons from lignin in Na-ion batteries

Source	Pre-treatment	Carbonisation	Surface area ($m^2\ g^{-1}$)	Electrode	Electrolyte	ICE	Capacity (mA h g^{-1})	Ref.
Oak sawdust	1. H_2SO_4	N_2 100 mL min^{-1}	208	10% AB	1 M $NaClO_4$ EC/PC/DMC (9 : 9 : 2)	68%	297 (50 mA g^{-1})	118
	2. KOH 3. HCl	1300 °C (6 h) 10 °C min^{-1}		20% PVDF			116 (2.5 A g^{-1})	
Peanut shell	H_3PO_4 (80 wt%)	Ar 1100 °C (1 h) 1 °C min^{-1}	30	10% C45 10% CMC (3-electrode)	1 M $NaClO_4$ EC/PC	68%	298 (20 mA g^{-1}) 77 (2 A g^{-1})	111
Cocoa pod husk	1 M HCl 60 °C 24 h	N_2 100 mL min^{-1} 1300 °C 5 °C min^{-1}	118 (47% mesopores)	10% AB 20% PVDF	1 M $NaClO_4$ EC/PC/DMC (9 : 9 : 2)	87%	317 (50 mA g^{-1}) 134 (250 mA g^{-1})	119
Phenolic resin + lignin (30 : 70)	No pre-treatment	Ar 1400 °C (2 h)	2.3	5% Na alginate	1 M $NaPF_6$ EC/DMC (1 : 1)	88%	373 (30 mA g^{-1}) 250 (300 mA g^{-1})	137
Alkali lignin	Pre-oxidation: air 200 °C (24 h) 5 °C min^{-1}	Ar 1350 °C (2 h) 2 °C min^{-1}	31	5% CB 5% Na alginate	1 M $NaClO_4$ PC 1 M $NaPF_6$ DEGDME	81.4% 86%	285 (50 mA g^{-1}) 175 (250 mA g^{-1}) 331 (50 mA g^{-1}) 307 (250 mA g^{-1})	112
Pitch	Pre-oxidation: air 300 °C (3 h)	Ar 1400 °C (2 h)	n/a	5% Na alginate	1 M $NaPF_6$ ED/DMC (1 : 1)	88.6%	301 (30 mA g^{-1}) ~250 (150 mA g^{-1})	113
Kraft lignin	Stabilisation Air 10 L min^{-1} 250 °C (30 min) 0.5 °C min^{-1}	N_2 0.3 L min^{-1} 1200 °C (20 min) 5 °C min^{-1}	94	Free standing electrode	0.6 M $NaPF_6$ DEGDME	89%	310 (30 mA g^{-1})	120
Lignin + epoxy resin (1 : 1 wt)	Air 150 °C (24 h)	Ar 1400 °C (1 h) 2 °C min^{-1}	n/a	5% Na alginate	0.8 M $NaPF_6$ EC/DME (1 : 1)	82%	316 (30 mA g^{-1}) 161 (300 mA g^{-1})	138
Lignin	Hydrothermal process + 3-aminophenol (11 wt%) 250 °C (12 h)	N_2 1100 °C (2 h)	727 (CO_2) 151 (N_2)	10% CB 2% CMC 3% SBR	1 M $NaClO_4$ EC/DEC (1 : 1)	85%	~325 (50 mA g^{-1}) ~150 (250 mA g^{-1})	122
Lignin	Hydrothermal treatment with GO and ethylene glycol 180 °C (20 h)	Ar 750 °C (2 h)	94	15% CB 10% PVDF	1 M $NaClO_4$ EC/DEC (1 : 1)	n/a	~210 (200 mA g^{-1})	131
Lignin sulfonate	Spray dried; Ar 500 °C (3 h) 1.2 M HCl	Ar 1300 °C (2 h)	12	10% AB 5% CMC 5% SBR	1 M $NaClO_4$ EC/DEC (1 : 1)	88.3%	339 (0.1C) 187 (1C)	139
Phenolic resin	Air 300 °C (3 h)	Ar 1300 °C (4 h)	47	5% Super P 5% PVDF	1 M $NaPF_6$ EC/DEC (1 : 1) + 5% FEC	76.4%	~315 (20 mA g^{-1}) ~75 (200 mA g^{-1})	114
Alkali lignin + PVA	Electrospinning with KOH (5 wt%)	Ar 600 °C (1 h)	93	Free-standing	1 M $NaClO_4$ EC/DMC (1 : 1) + 5 wt% FEC	65%	137 (50 mA g^{-1}) 87 (300 mA g^{-1})	140
Corn stalk	Purification (acetone); composite with amphiphilic carbonaceous material	N_2 400 °C (1 h) H_2/Ar 1300 °C (3 h)	5.3	10% super P 10% PVDF	1 M $NaClO_4$ EC/DEC (1 : 1)	82%	297 (25 mA g^{-1}) ~160 (200 mA g^{-1})	141
Lignin	Washing with KOH (20 wt%) and HCl (1 M)	N_2 100 mL min^{-1} 1300 °C (6 h) 5 °C min^{-1}	48	10% AB 20% PVDF	1 M $NaClO_4$ EC/PC/DMC (9 : 9 : 2)	69%	~270 (50 mA g^{-1}) ~175 (250 mA g^{-1})	117

Table 2 *(Contd.)*

Source	Pre-treatment	Carbonisation	Surface area (m^2 g^{-1})	Electrode	Electrolyte	ICE	Capacity (mA h g^{-1})	Ref.
Lignin sulphonates	Ar	Ar	5.6 (N_2)	10% carbon SP	1 M $NaClO_4$ EC/DMC	79%	270 (25 mA g^{-1})	115
	600 °C (1 h) Water washing	1200 °C (1 h) 5 °C min^{-1}	377 (CO_2)	10% CMC				
Scrap wood	Washing with 1 M H_2SO_4	Ar 20 mL min^{-1} 1000 °C (6 h) 13 °C min^{-1}	30	10% CMC	1 M $NaPF_6$ EM/DEC (1 : 1)	86%	270 (30 mA g^{-1})	116
Pitch + lignin	—	Ar	1.3	5% Na alginate	0.6 M $NaPF_6$ EC/DMC (1 : 1)	82%	254 (0.1C)	142
		1400 °C (2 h)						
Lignin	Washing with HCl + formaldehyde	N_2	16	10% Super P	1 M $NaClO_4$ EC/DEC (1 : 1) 5% FEC	74%	325 (25 mA g^{-1}) 140 (250 mA g^{-1})	143
		2 °C min^{-1} 400 °C (1 h) 5 °C min^{-1} 1300 °C (1 h)		10% PVDF				
Lignin + PAN (5 : 5)	Air	N_2	26.6	Free standing	1 M $NaClO_4$ EC/DEC (1 : 1)	70.5%	296 (20 mA g^{-1}) 80 (1 A g^{-1})	144
	400 °C (1 h)	1300 °C (0.5 h)						
Lignin from corn stalks	Extraction with acetone (purification)	N_2	14	10% Super P	1 M $NaClO_4$ EC/DEC (1 : 1)	79%	~300 (50)	145
	+20% $(NH_4)_2HPO_4$	(1) 400 °C (1 h) (2) 1300 °C (2 h)		10% PVDF			~160 (50)	
Alkali lignin derived AZO polymer	Formation of composite with SiO_2, later removed with HF	N_2	449.7	10% CB	1 M $NaClO_4$ EC/DMC (1 : 1)	50%	190 (50 mA g^{-1})	146
		5 °C min^{-1} 700 °C (4 h)		10% CMC			161 (200 mA g^{-1})	
Cocklebur fruit	Soaking in $NH_3 \cdot H_2O$	1100 °C (3 h)	64	10% super P	1 M NaOTf DEGDME	69%	253 (50)	121
				10% PVDF			106 (1 A g^{-1})	
Lignin + 3-aminophenol formaldehyde resin (3 : 7)	—	Ar	18.4	10% GVXC-72	1 M $NaClO_4$ EC/DEC (1 : 1)	81%	310.4 (25 mA g^{-1})	123
		1100 °C (2 h)		5% CMC			125 (200 mA g^{-1})	
Alkaline lignin + melamine + urea (1 : 1 : 5)	Formation of composite	N_2	n/a	10% Ketjen black	1 M $NaPF_6$ EC/DEC (1 : 1)	26%	247 (30 mA g^{-1})	125
		5 °C min^{-1} 400 °C (2 h) 800 °C (4 h)		10% CB 10% PTFE			167.1 (300 mA g^{-1})	
Enzymatic lignin	Water washing	Ar	4		1 M $NaPF_6$ DEGDME	74.4%	303 mA g^{-1} (100 mA g^{-1}) ~260 (400 mA g^{-1})	147
		5 °C min^{-1} 1600 °C (2 h)						

than LIBs (~260 W h kg^{-1}) and are broadly researched worldwide.[148–150] However, S, as a cathode material exhibits low conductivity (requiring conducting additives) and a large volume expansion during cycling that is detrimental to battery life.[151–153] The gradual leakage of active material due to the polysulfide "shuttle" effect further leads to capacity decay and short cycle life.[149] Lignin derived carbons can have a significant impact on the performance when applied as hosts/conductive additives for S-cathodes in LSBs. The S can be effectively impregnated within the conductive matrix of porous carbon to enhance the cycling stability. Conductive porous carbon scaffolds not only increase the surface area to boost sulphur loading compared to non-porous hosts but significantly enhance the electrical conductivity and limit polysulfide diffusion during cycling. Shen *et al.*,[154] for example, developed a lignin based porous carbon with a high surface area (1211.6 m^2 g^{-1}) and oxygen-containing surface functional groups that enabled high S-loading (50 wt%), leading to increased capacity (1330.7 mA h g^{-1}) and high initial CE (81.3%). However, the capacity retention was 62.6% after only 100 cycles, suggesting that the polysulfide diffusion was not adequately suppressed, thus, further strategies are needed to enhance the electrode performance. By doping N into a lignin-derived porous carbon nanosphere matrix, Liu *et al.*[155] achieved a suppressed polysulfide shuttling effect, allowing the anode to achieve a long life of over 1000 cycles at 1.0 C with a capacity decay of only 0.041% per cycle. The task of future research should be more focused on developing lignin

materials with the capacity to effectively host S and suppress the shuttling effect. This requires rational nanoengineering and efficient synthesis techniques tailored at addressing the huge volumetric expansion issues rather than focusing only on porous architectures and continuous S-loading. Another key challenge hindering the viable commercial deployment of LSBs is polysulfide dissolution in the electrolyte which often leads to poor reversibility and long-term cycling performance limitations. Selective material coating approaches have been proposed to resolve this issue in other S-hosting materials but rarely are investigated for with lignin-based cathodes. Most reports focused on the high surface area of lignin derived electrodes in LSBs and LIBs. This however often leads to low initial CE due to collapse of the micropores in the carbon framework. Therefore, the pore-inducing carbonization process should be regulated to tune the pore distribution and surface area for optimum S-loading while also enhancing the conductivity to improve the cell performance characteristics such as CE and rate capability.

2.2.2. Metal–air batteries cathodes. The high theoretical capacity, low cost and relative high safety of metal–air batteries such as Li–O_2 batteries (LOBs, 3500 W h kg^{-1}) and Zn–air batteries (ZABs, 1353 W h kg^{-1}, excluding oxygen) make them attractive energy storage devices.[156,157] However, the practical energy density of LOBs is limited by the inherent insulating properties of the lithium peroxide (Li_2O_2) generated during cycling. An alkaline lignin-derived porous carbon cathode with a high surface area (1961 m^2 g^{-1}) and abundant defect sites for LOBs delivered superior capacity (7.2 mA h cm^{-2}) and a long cycle life of over 300 cycles[158] compared to commercial carbon materials such as Super P and KB.[158,159] Li *et al.*[160] designed a high surface area (782 m^2 g^{-1}) lignin-derived Fe, N, P, S co-doped porous carbon composite cathode for ZABs that achieved an open-circuit voltage of 1.49 V and a discharge capacity of 729.2 mA h g^{-1}. These reports further reveal the potential of lignin as a precursor material for a broad range of battery cathodes. The insulating properties of Li_2O_2 remains a challenge in LOB regardless of the cathode design, thus, strategies to overcome this problem remain unresolved and must be pursued in future studies. Formulating an electrolyte with the desirable properties (high stability/low decomposition, non-toxicity, low volatility, wide electrochemical window stability, and a high rate of oxygen solubility) also remains a big barrier in metal–air batteries (MABs). These need to be addressed with a focus on tailoring the chemical structure and surface reactivity of the cathodes to minimise these issues without sacrificing the capacity. Carbon materials are typically unstable above 3.5 V which exacerbates the side reactions problem and remains a critical issue to be addressed. It would be useful to address these barriers on several fronts such as through nanoengineering and functionalisation with secondary materials, and to explore side reaction and passivation layer inhibitors. Future studies on electrolyte chemistries specifically tailored for enhanced redox reactivity/stability, high oxygen solubility, high ionic conductivity, and reduced rate of passivation layer formation compatible with the lignin-based cathodes for high energy density delivery is highly recommended. The typical operation of MABs in an open system can also lead to parasitic reactions due to electrode contamination from atmospheric moisture and gases (*e.g.*, CO_2, N_2, organic vapours, *etc.*) which can undermine the advances made on the cathode and electrolyte development. This should be tackled from the packing engineering level to limit atmospheric interference without inhibiting oxygen flow, and at the electrode and electrolyte level using inhibitors or selective adsorbents.

2.3. Lignin based binders

The primary role of binders (typically 2–5 wt% of the electrode) is to ensure an excellent mechanical adhesion and stability of the electrode active materials by maintaining uniformity and intimate contact between active material constituents, conductive additives and the current collector (electrode coating). These features render binders critical to battery safety, cycle life and capacity retention. Traditional binders such as polyvinylidene fluoride (PVDF) require expensive and toxic organic solvents (*e.g.*, *N*-methyl-2-pyrrolidinone and acetonitrile), necessitating demands for greener, sustainable and less expensive alternatives.[81,161,162] In this regard, binders that are dispersible in water (*e.g.*, poly(tetrafluoroethylene, tapioca starch and carboxymethyl cellulose) have been developed recently.[81,161,162] Lignin is a good binder material as it satisfies all the above binder requirements in addition to eco-friendliness, abundance and good thermal stability. In particular, the ample functional groups of lignin make it easy for surface modification and functional tailoring of its properties. Moreover, its highly cross-linked structure is suitable for achieving mechanically robust adhesion while the polar functional groups render it hydrophilic, making it processable in aqueous solvents which is suitable for green battery production. Cheng's group[163] for example demonstrated that lignin could act as a binder for Si NPs and be subsequently converted at 400–800 °C into a conductive ligament. This allowed for designing a mechanically robust Si/carbon composite electrode free of traditional binders with enhanced electrochemical stability for over 250 cycles compared to a PVDF binder. Luo *et al.*[164] also developed a water-soluble binder consisting of sodium polyacrylate grafted lignin for micro silicon anodes *via* free radical graft copolymerisation and alkaline hydrolysis. The anode exhibited high performance stability against the high volumetric changes of Si for over 100 cycles compared to that using a CMC binder. Lignin binders with additional capabilities for specific functions have also been explored for LSBs, including a sodium lignosulfonate salts-based binder containing negatively charged sulfonate groups that are beneficial for suppression of lithium polysulfide diffusion, thus, allowing stable cycling performance for 100 cycles at 0.2 C. The rich phenolic groups in lignin have also been exploited as a free radical scavenger in $LiNi_{0.5}Mn_{1.5}O_4$ cathode based high voltage LIB which suppressed the free radical chain reaction, allowing for the generation of a compatible multi-dimensional interphase between the electrolyte

and electrode. This enabled the electrode to maintain high stability with high capacity retention (94.1%) after 1000 cycles compared to that of a PVDF (46.2%).[165] Although the study of lignin based binders is still at the infancy stage, a critical issue to be resolved is that by thermally converting the lignin binder into an active carbon ligament within the electrode, the robustness may be severely diminished during the charge/discharge due to repeated expansion/contraction and structural changes, however minimal, which can compromise the mechanical functions of the binder in the electrode and lead to capacity decay and poor cell performance. The use of unconverted lignin extracts as binders could also pose the challenge of low conductivity and dead mass in addition to increased parasitic reactions by the surface functional groups or the added structure-improving polymers and lead to rapid electrolyte decomposition and consumption which are undesirable in practical batteries. Therefore, detailed electrochemical studies of the lignin binder redox behaviour and stability mechanism with respect to the electrode structure and cycling characteristics is needed. Furthermore, all conventional binders do not always function adequately with all kinds of electrode materials in different cell types, thus, it will be useful to undertake rigorous electrochemical screening to identify the most suitable combinations and cycling conditions for their application in various battery systems.

2.4. Integration of lignin in electrolytes and separators

The leakage, gas evolution, flammability and toxicity of the organic liquid electrolytes are serious safety concerns in the operation of batteries. Such issues are limited to a large extinct in gel polymer electrolytes (GPEs) although hazardous polymers are still used.[166] The demand for "green batteries" requires the exploration of natural biodegradable polymers for GPEs. While lignin as a natural material cannot be used in batteries as an electrolyte, its porous derivates (composite, films, membranes, nanofiber mats, *etc.*) can be utilized for preparing durable, flexible, and resilient GPEs. These lignin-derived porous structures serve as mechanical supports that can absorb a particular activating agent (liquid electrolytes) and serve as electrolytes in rechargeable batteries. Water-soluble lignin has been thoroughly mixed with poly(*N*-vinylimidazole)-*co*-poly(poly (ethylene glycol) methyl ether methacrylate) copolymer (weight ratio of 2 : 1) for three days to develop a lignin-based thin film. An organic liquid electrolyte was used for activating the lignin-based film before its use as a Li-ion battery electrode. This synthesized GPE suppressed Li dendrite formation in a Li metal anode and maintained adequate ionic conductivity (6.3×10^{-4} S cm^{-1}). Moreover, this arrangement resulted in a stable performance (~150 mA h g^{-1}) for over 450 cycles at 1C in a Li/$LiFePO_4$ cell.[166] The acidity of fumed silica in the GPE was reduced by blending with lignin to develop a GPE for rechargeable aqueous Zn/$LiMn_2O_4$ batteries, that exhibited improved stability of electrochemical properties.[166] The acidity of fumed silica in the GPE was reduced by blending with lignin to develop a GPE for rechargeable aqueous Zn/$LiMn_2O_4$ batteries, that exhibited improved stability of electrochemical properties.

Lignin also exhibits potential for use in the development of solid polymer electrolytes (SPEs). Liu *et al.* successfully developed lignin derivatives for use as a SPE in Li–metal batteries. Softwood kraft lignin was dissolved in organic solvent (dimethylformamide (DMF)) and its chemical structure was modified into abundant alkene group *via* esterification reactions with *N*,*N*′ dicyclohexylcarbodiimide, and 4-(dimethylamino)pyridine. Lignin-based SPE was formed by graft-copolymerisation of poly(ethylene glycol)(PEG) with lignin–alkene *via* a photoredox thiolene reaction (*i.e.*, grafting and crosslinking reaction procedures). Newly synthesized lignin-*graft*-PEG combines the mechanical and thermal properties of lignin with the flexibility and superior ionic conductivity of PEG.[167] The solid electrolytes served as a binder and an ion conductor with the capability of suppressing dendrite formation. While all these findings show high promise for lignin, the requirement of synthetic polymer blends dilutes the eco-friendliness and performance of the lignin-based battery component. Nonetheless the results in the literature to date show that lignin is a promising material for battery electrolyte development.

Meanwhile, the safety of rechargeable batteries hinges on the separator, which is typically a polymeric membrane that must be chemically and electrochemically stable and compatible with the electrolyte and electrode materials and mechanically robust enough to endure any stress that occurs during battery assembly.[168] Similar to binders, the structure and properties of the separator significantly affect the energy and power density, safety and cycle life of the battery. Traditional separators are made of polyolefins (polypropylene, polyethylene, polyisobutylene and polymethylpentene) with semi-crystalline structures.[169] The polyethylene backbone is often grafted with micro-porous poly(methyl methacrylate) or siloxane to improve performance. Lignin based separators combine high performance with abundance and environmental benignity. For example, the introduction of lignin in organic polymers such as poly(vinyl alcohol) or polyacrylonitrile (PAN) in separators resulted in improved porosity, high electrolyte wettability, improved thermal stability and enhanced ion transport. Zhao *et al.* employed electrospinning of lignin/polyacrylonitrile solution to prepare a composite fibre-based nonwoven separator. Various amounts of lignin were dispersed in organic aqueous mixtures (PAN–DMF) under continuous mechanical stirring to prepare lignin/PAN solutions. The synthesized separator resulted a remarkably stable cell performance of a Li/$LiFePO_4$ cell with a capacity of ≈148.9 mA h g^{-1} after 50 cycles at 0.2 °C for the lignin–PAN (3 : 7 wt/wt) compared to commercial Celgard-2400 (≈132 mA h g^{-1}) at the same rate.[170] While these preliminary studies show high promise for lignin derived GPE and solid-state electrolytes, their performance is still limited and far from meeting practical application requirements. Thus, further improvements are needed to enhance the conductivity and compatibility with other cell components. The literatures surveyed suggest that most studies are conducted at room temperature. This should be expanded to at least the −20 °C to 60 °C range with further analysis of the impact of structural properties on the viscosity, decomposition and conductivity. The separator

also needs to be designed with an adequate balance of the required properties such as conductivity, wettability, and porosity, and sufficiently thin with excellent mechanical robustness. Thus, it is recommended to improve the mechanical and electrical properties of both separator and electrolyte to a level equivalent and/or exceeding the state of the art to become practically viable. This will also require advanced characterization tools for *operando* and *in situ* analysis in both half and full cell testing and analysis under practical conditions.

2.5. Redox flow batteries

Research to date has shown that lignin, a cheap, abundant and renewable material, can be applied to all of the main components of a redox-flow battery (RFB). Carbon fibres produced by electrospinning of lignin have been employed as electrodes in a vanadium RFB. Unlike in metal-ion batteries where the electrode material is electrochemically active, electrodes in redox-flow systems simply have the purpose of supplying active sites for the redox reaction of electroactive species in the electrolytes. Most electrode materials in these systems are carbon cloths, felts, or papers from non-renewable sources,[171] so producing carbon from biomass such as lignin is a positive step towards sustainable redox-flow batteries. Ribadeneyra *et al.* produced carbon fibres from electrospinning a lignin solution.[172] After a two-step carbonisation, the high surface area electrodes showed inferior performance to carbon paper in a full cell, but good activity in a vanadium RFB half-cell. The successful use of the electrospun carbon fibres from lignin could be a matter of optimizing electrode processing and more research is necessary.[171]

The beneficial properties of lignin have also been exploited in the development of RFB ion exchange membranes. To separate the anolyte and catholyte in vanadium RFBs, lignin composite membranes with a sulfonated poly(ether ether ketone)[173] or Nafion polymers[174] were designed by Ye and coworkers. The latter composite membrane presented better performance with higher coulombic efficiency and capacity retention (97.4% and 52.8%, respectively) than the pure Nafion membranes (90% and 34.8%, respectively). Besides the promising application of lignin in RFB electrodes and membranes, the biopolymer has also been investigated as source material for redox-active organic molecules in RFBs. Commonly used active species include expensive metals such as vanadium and chromium, but organic molecules could be a viable option. Mukhopadhyay *et al.* used lignosulfonate directly derived from lignin as anolyte,[175] showing that lignin is not only a viable material to produce electrode materials and separators, but also electrolytes. Redox flow batteries are a promising technology gaining space in the market, but the use of lignin as a precursor or directly as a component is still incipient.

3. Lignin for energy applications – supercapacitors

Commercial electrical double layer capacitors (EDLCs), also known as supercapacitors, store charge using two symmetrical porous activated carbon electrodes in an organic electrolyte. The electrode makes up 28% of the cost of commercial supercapacitors, with 39% of that attributed to the cost of activated carbon (10–20 EUR kg^{-1}) and 59% to the cost of the current collector (foil).[176] Thus, there is significant scope to replace the activated carbon with carbon materials synthesised from lignin, due to lignin's high carbon content (~60%) and lower cost. The 3D polymeric nature of lignin also provides unique advantages over traditional activated carbon to enhance performance and reduce costs. It can be templated, form hydrogels and aerogels, combined with pseudocapacitive materials and spun into free-standing flexible fibre electrodes.[177–182] The most common methods used to produce lignin-based carbon electrodes for supercapacitor applications are shown in Fig. 4. The free-standing electrodes have the potential to remove the need for a current collector, simplifying the cell and further reducing environmental and commercial costs for supercapacitors.

3.1. Activated carbon lignin electrodes for EDLCs

Activated carbons are highly porous materials with a high specific surface area (SSA, >1500 $m^2\ g^{-1}$), reasonable electrical conductivity (0.39 cm^{-1} for Norit Super 30 and 0.74 S cm^{-1} for Kansai Maxsorb),[183] and low cost compared to other supercapacitor materials (*e.g.*, graphene RuO_2). The high SSA of these materials is critical for energy storage in EDLCs, as capacitance is governed by the degree of surface area electrostatically interacting with the electrolyte. Early efforts to generate activated carbon from lignin started in the 1970s for adsorption applications,[184] but it was not until the 2010s when lignin based supercapacitors appeared.[185] These initial adsorption studies demonstrated that temperature, residence time, activation agent and ratio, as well as the type of lignin all influence the properties of the final activated carbon product.[184] Applying this knowledge to supercapacitors, Jianhui *et al.* demonstrated that the capacitance of KOH activated lignin (900 °C, 1.5 h) could be improved from 196.1 to 267.8 F g^{-1} (0.05 A g^{-1}, 6 M KOH/LiOH, 1 V window) by adjusting the KOH : lignin ratio from 1 : 1 to 3 : 1. This was attributed to the increase in SSA from 718 to 1506 $m^2\ g^{-1}$.

The different physicochemical properties of various lignin derivatives resulting from their diverse extraction and growing conditions is a major issue for commercializing lignin. Li *et al.* examined the EDLC performance of activated carbon from extracted lignin from pine (softwood) and poplar (hardwood). The pine lignin exhibited a specific capacitance of 48.3 F g^{-1}, while poplar lignin was 86.7 F g^{-1} (0.5 A g^{-1}, 1 M H_2SO_4, 0.6 V window). The higher performance of poplar lignin was attributed to its higher SSA (621 *vs.* 314 $m^2\ g^{-1}$) after activation resulting from the difference in G and S units between the pine (softwood, only G units) and popular (hardwood, G and S units). It should be noted that the activation temperature in this study (700 °C) is lower than what is commonly used for KOH activation (800–900 °C) and may have resulted in their lower performance. Similarly, Du *et al.* compared the storage capacity of carbon derived from hardwood (poplar), soft-

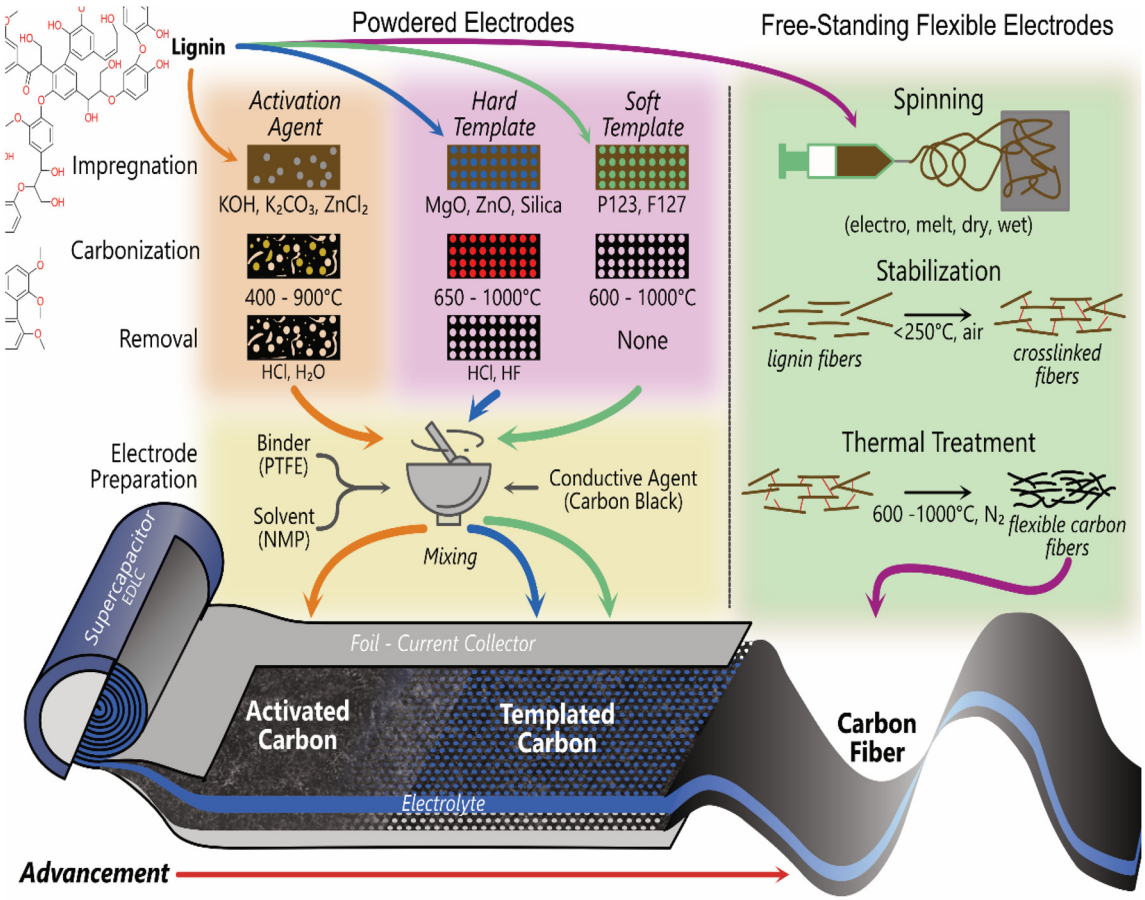

Fig. 4 Main methods used to produce carbon electrodes from lignin for supercapacitors.

wood (pine) and grass (corn stover). Poplar based carbon had an increased surface area of 1062.5 m^2 g^{-1} and specific capacitance of 349.2 F g^{-1} (0.1 A g^{-1}, 6 M KOH, 1 V window). Du attributed the increased performances to the increased amount of S units and larger molecular weight.[186]

Pursuing the highest surface area was the goal of many studies to increase the capacitance of lignin-based supercapacitors. Yu *et al.* demonstrated that incorporating a pre-pyrolysis step (600 °C, 1 h, N_2) before activation (3 : 1 KOH, 800 °C, 2 h, N_2) increased the gravimetric capacitance from 218 F g^{-1} to 312 F g^{-1} (0.05 A g^{-1}, 6 M KOH, 1 V window).[187] This was attributed to the increase in the V_{micro}/V_{total} ratio from 22% to 66%. Hydrothermal carbonisation can also be used as a pre-carbonisation step (Fig. 5a).[188,189] Guo *et al.* hydrothermally carbonized enzymatic hydrolysis lignin at 180 °C in 5% wt H_2SO_4 for 18 hours before activating the resultant carbon product with KOH at different ratios (800 °C, 3 h, N_2).[189] They achieved a specific capacitance of 420 F g^{-1} in 6 M KOH (0.1 A g^{-1}, 1 V window) and 218 F g^{-1} in neat EMIM TFSI (1 A g^{-1}, 2.5 V window). The high performance of their carbon was attributed to the combination of micro (0.66 cm^3 g^{-1}) and mesoporosity (0.10 cm^3 g^{-1}) formed in the two-step process and not just the high SSA (1660 m^2 g^{-1}). Thus, to achieve the highest surface areas and pore distributions, most studies have adopted a two-step activation method with a pre-carbonisation step.[189–193]

One of the issues with activated carbon production is the use of highly corrosive (*e.g.*, KOH,[185,187,190–199] NaOH,[196,200] H_3PO_4 [201]) or toxic ($ZnCl_2$ [202]) activation agents for enhancing the surface area and porosity in lignin. Fortunately, efforts are being made to shift towards greener activation agents and methods. For example, Schneidermann *et al.* demonstrated that ball milling lignin with K_2CO_3 and urea before thermal treatment at 800 °C achieved a SSA of 3041 m^2 g^{-1}. This material had a specific capacitance of 177, 147, 192 F g^{-1} in 1 M Li_2SO_4, 1 M TEA–BF_4 and EMIM–BF_4 at 0.1 A g^{-1}. Alternatively, Jeon *et al.* applied a different approach examining the self-activation of lignin by thermal treatment without activation agent. A SSA of 1092 m^2 g^{-1} was achieved on a purified Kraft lignin attaining a capacitance of 91 F g^{-1} (0.5 A g^{-1}, 1 M H_2SO_4, 1 V window). Liu *et al.* achieved higher capacitance values by freeze drying alkali lignin before the carbonisation step, negating the need for an activation agent. The resultant carbon had a SSA of 854.7 m^2 g^{-1} and a specific capacitance of 281 F g^{-1} (0.5 A g^{-1}, 1 M H_2SO_4, 1 V window). These studies reveal that greener activated carbons can be created with lignin using more sustainable activation agents or agent-free methods.

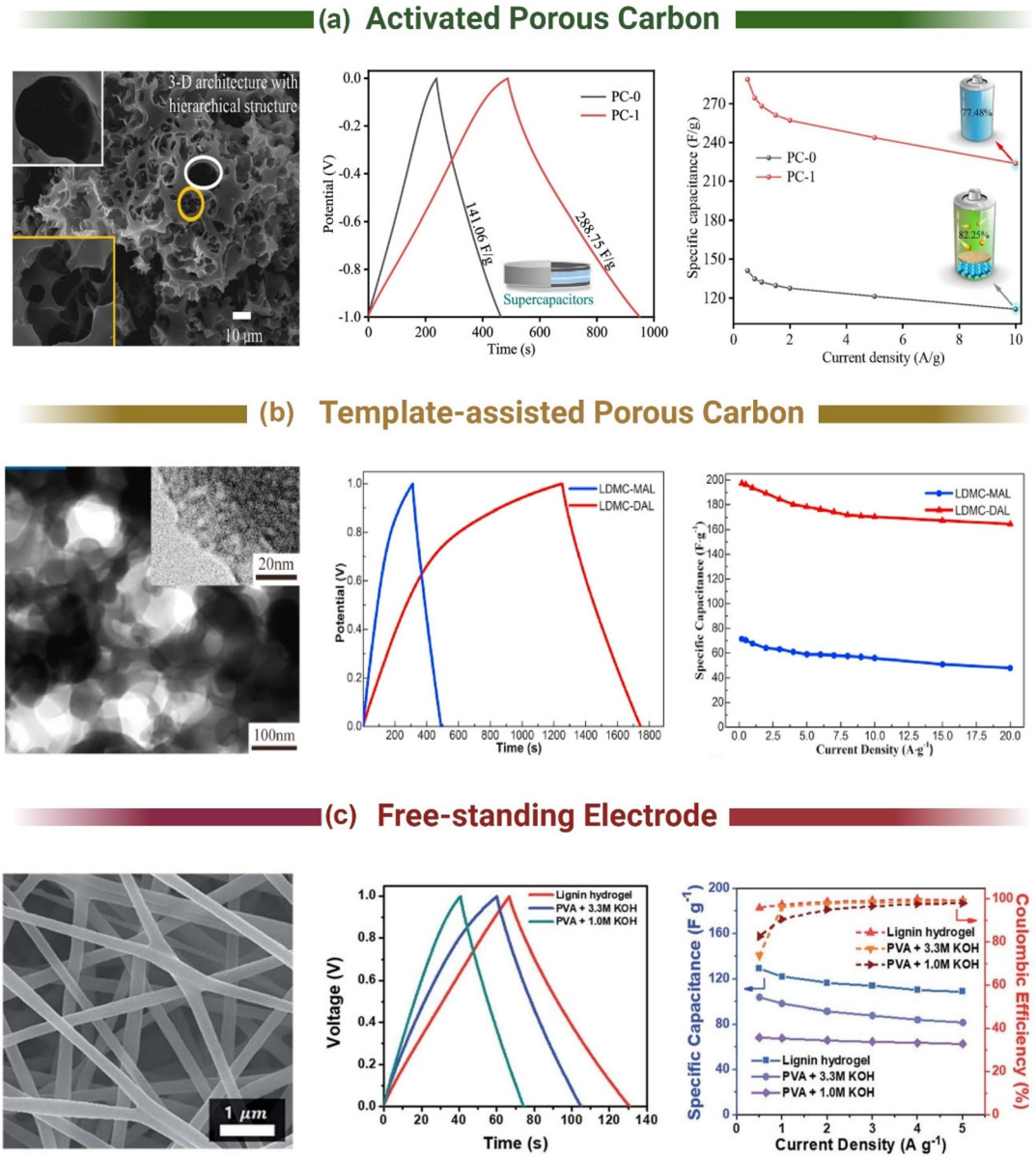

Fig. 5 Morphology and electrochemical performance of Lignin-derived carbon materials for supercapacitor applications using (a) activated porous carbon. Adapted with permission from ref. 188. Copyright 2021, American Chemical Society (b) template-assisted porous carbon. Adapted with permission from ref. 213. Copyright 2021, Elsevier and (c) flexible free-standing conductive carbon electrodes. Adapted with permission from ref. 217. Copyright 2019, Royal Society of Chemistry.

Increasing the surface area of activated carbons has been the main method of enhancing EDLC performance. Recently, it has become evident that pore size and carbon nanostructure are more crucial in increasing specific capacitance than raw surface area. This can be seen when comparing the results in the previous examples where the relationship between SSA and performance is not linear.[185,187,189] As it is difficult to tailor activated carbons towards specific porous structures, researchers have attempted to create tailored carbon materials with specific nanostructures to enhance the energy density of lignin-based supercapacitors.

3.2. Templated porous carbon materials from lignin

Template methods using soft or hard templates (porogens) allow the creation of highly tailorable pore size distributions in carbon materials. Hard templating consists of impregnating inorganic compounds into the lignin structure, such as MgO,[203] ZnO,[204] silica,[205,206] and zeolites,[207,208] which are removed after thermal treatment to leave pores in the carbon matrix. For instance, Tain *et al.* used sodium lignosulfate and tetraethyl orthosilicate as a silica template to create a mesoporous sulphur doped carbon structure. The silica template

was removed with 40% HF, resulting in a SSA of 1054 $m^2 g^{-1}$ and an average pore diameter of 6.69 nm. This material achieved a capacitance of 241 F g^{-1} (1 A g^{-1}, 6 M KOH, 1 V window).[209] The use of toxic or corrosive compounds (*e.g.*, HF[206,209]) is a problem in hard templating and undermines the environmental benefit of using lignin. To address this, Fu *et al.* combined sodium lignosulfonate, $Zn(NO_3)_2{\cdot}6H_2O$, $Na_2C_2O_4$ and ethanol to form a self-assembled lignin/ZnC_2O_4 composite. This composite was carbonized at 650 °C creating a lignin/ZnO hybrid with porosity formed by removing the nano-sized ZnO template with 1 M HCl. The removal of ZnO created a mesoporous material (12.9% V_{micro}/87.1% V_{meso}) with a specific capacitance of 274 F g^{-1} at 0.5 A g^{-1} and 200 F g^{-1} at 20 A g^{-1} in 6 M KOH (1 V window). Although they avoided using toxic or corrosive activation agents to create porosity, the removal of ZnO with HCl is likely to create aqueous $ZnCl_2$, which is toxic to aquatic and plant life.[210–212]

Soft templating methods using polymers and surfactants solve the template removal issue as the template is consumed during the thermal treatment step. For example, Herou *et al.* demonstrated the green synthesis of mesoporous carbon from organosolv lignin using phloroglucinol, glyoxal and F127 surfactant. The phloroglucinol and the lignin self-assembled around F127 micelles with the glyoxal acting as a cross-linker to form an evaporation-induced self-assembled structure. Subsequent carbonisation at 900 °C resulted in a mesoporous structure with a SSA of 763 $m^2 g^{-1}$ and a specific capacitance of 90 F g^{-1} (0.1 A g^{-1}, 6 M KOH, 1.2 V window).[179] Unfortunately, the low SSA of soft templated carbons tend to hinder their performance in supercapacitors, which has been addressed by combining templating methods with either pre-treatment or post-treatment methods. Sima *et al.* performed a pre-treatment on lignin using a choline chloride/formic acid based deep eutectic salt before soft templating with F127 (Fig. 5b).[213] The deep eutectic salt treatment created an ordered mesoporous carbon, increased the SSA by 56% to 1195 $m^2 g^{-1}$ and more than doubled the pore volume (0.7 $cm^3 g^{-1}$). This improved the specific capacitance from ~72 F g^{-1} (0.2 A g^{-1}, 6 M KOH, 1.0 V) in the untreated sample to 197.32 F g^{-1} (0.2 A g^{-1}, 6 M KOH, 1.0 V) for the pre-treated material. Post treatment of templated carbons typically involves employing activation agents to increase the microporosity in the generally mesoporous structure created from templating. For instance, Saha *et al.* combined hard wood Kraft lignin with Pluronic F127 and carbonized at 1000 °C to create a mesoporous carbon.[214] This material exhibited a SSA of 185 $m^2 g^{-1}$, resulting in a specific capacitance of 77.1 F g^{-1} (1 mV s^{-1}, 6 M KOH, 0.8 V window). To improve the performance, the templated carbon was activated with CO_2 or KOH. This increased the specific capacitance to 91.7 F g^{-1} for CO_2 activation and 102.3 F g^{-1} for KOH. Finally, a few studies also state a template-free method of creating porous carbon by utilizing a slurry of KOH/lignin before thermal treatment.[199,215,216] However, this is more akin to the traditional activation method and still requires a post washing step to remove any residual materials.

Templating methods allow a high level of control over the porosity in carbon materials, allowing the formation of hereti-cal porous carbons matched to the electrolyte. However, these materials tend to be powdered requiring them to be mixed with binders (PTFE), conductive agents (carbon black) and attached to a current collector/foil to form an electrode. These extra components increase the size of the device and are a source of resistive interfaces between the active material and the current collector. Replacing powdered materials with electrically conductive free-standing electrodes provides the opportunity to omit these components, reducing the complexity and increasing the volumetric capacity.

3.3. Flexible free-standing electrically conductive electrodes

Development of lignin based flexible free-standing electrodes is the next step in electrode design for supercapacitors. These electrodes are commonly synthesised from electrospinning,[218–221] melt spinning,[28,222,223] wet spinning,[224,225] gel spinning,[226] centrifugal spinning,[227] or dry spinning[228] the lignin into flexible carbon fibre mats (Fig. 6). In all these techniques, the precursor polymer is initially formed into fibres, followed by thermal treatment at high temperature (>600 °C) under inert atmospheres (N_2, Ar). An additional stabilisation step is typically included between spinning and carbonisation to convert the lignin polymer into a thermoset polymer. During this stage, the fibres are heated at a very slow rate (<1 °C min^{-1}) under an oxidative atmosphere until they reach 200 to 300 °C, where they are kept for several hours. Stabilisation is critical as it prevents morphological changes in the fibres when carbonized at high temperatures. Schlee *et al.* investigated the impact of stabilisation conditions on electrospun softwood and hardwood Kraft lignin.[229] Stabilizing at 190 °C created almost no structural changes in the lignin fibres, resulting in the hardwood Kraft lignin melting under carbonisation at 800 °C. At 250 °C, both types of lignin stabilized without fusing with increases in stabilisation temperature leading to higher SSA (918 $m^2 g^{-1}$ at 340 °C). However, this also led to increased mass loss during stabilisation. At 250 °C, 79.1% of the hardwood Kraft lignin remained after stabilisation which dropped to 36.5% after stabilisation at 340 °C. The hardwood Kraft lignin achieved a maximum specific capacitance of 164 F g^{-1} (0.1 A g^{-1}, 6 M KOH, 1.2 V) when stabilized at 310 °C, whereas the softwood Kraft lignin achieved 150 F g^{-1} (0.1 A g^{-1}, 6 M KOH, 1.2 V) when stabilized at 340 °C. The differences here were associated with the different side-chain linkages, functional groups and molar mass of the softwood and hardwood Kraft lignins, which in turn influence the stabilisation and final porosity of the carbon fibres.

It is possible to spin pure lignin solutions into carbon fibres,[230] but the low molecular weight of lignin makes this difficult. Thus, lignin is typically mixed with polymers, such as polyacrylonitrile (PAN),[217,220,231–233] Polyethylene Oxide (PEO),[177,178,234] and polyvinyl alcohol (PVA),[235–237] to increase the spinnability and enhance the properties of the fibres. Wang *et al.* created binder-free electrodes by electrospinning PAN and enzymatic hydrolysis lignin at different ratios.[220] The precursor mats were stabilized in air at 250 °C (1 °C min^{-1}) and carbonized at 800 °C (10 °C min^{-1}) under N_2. They found that a ratio of 40 : 60 PAN to lignin lead to the highest SSA (675 $m^2 g^{-1}$), which resulted in a specific capacitance of 216.8 F g^{-1} (1 A g^{-1}, 6 M

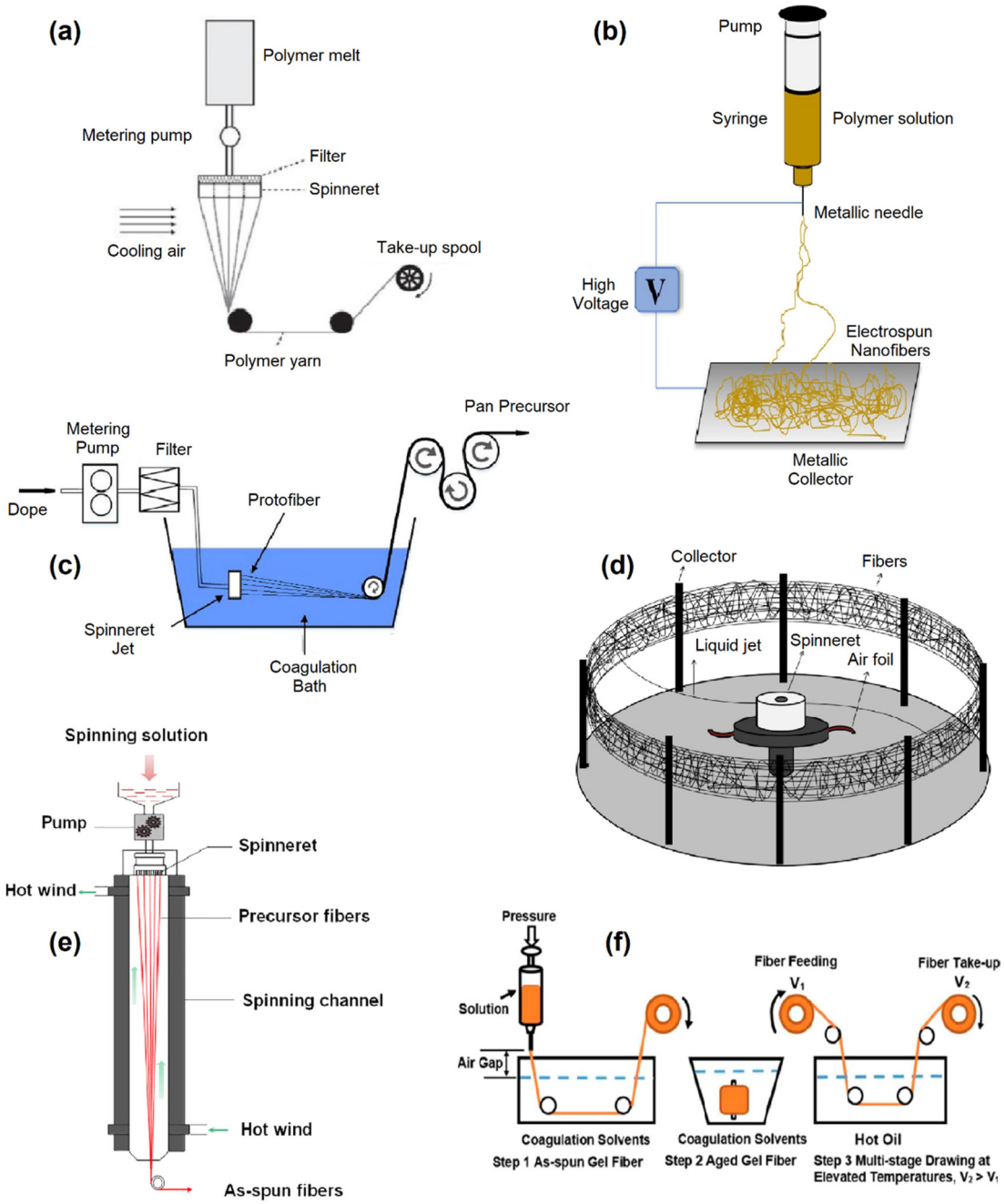

Fig. 6 Schematic representation of (a) electrospinning. Adapted with permission from ref. 218. Copyright 2020, American Chemical Society (b) melt spinning. Adapted with permission from ref. 222. Copyright 2021, MDPI (c) centrifugal spinning. Adapted with permission from ref. 227. Copyright 2015, MDPI (d) wet spinning. Adapted with permission from ref. 238. Copyright 2020, Elsevier (e) gel spinning. Adapted with permission from ref. 226. Copyright 2017, American Chemical Society (f) dry spinning. Adapted with permission from ref. 239. Copyright 2020, Wiely.

KOH, 1 V window). However, an issue with lignin spun fibres is beading,[235] where small beads of solution are deposited along the fibre length due to viscoelasticity of the lignin solution. Fang *et al.* addressed this by incorporating surfactants (0.2–1.2%) into the spun solution, which eliminated the beads and enhanced the orientation of the fibre microstructures. This in turn increased the specific capacitance from 66.3 to 80.7 F g^{-1} (1 A g^{-1}, 6 M KOH, 1 V window). Additionally, the sporadic nature of carbon fibres forming under spinning techniques also leads to large voids between the fibres, reducing their volumetric energy density. Herou *et al.* addressed this issue by compacting organosolv electrospun lignin fibres with uniaxial compression, reducing the inner-fibre pore size from 1–5 μm to 0.2–0.5 μm. This environmentally friendly and straightforward step, applied prior to carbonisation, improved the volumetric capacitance from 20 to 130 F cm^{-3} (0.1 A g^{-1}, 6 M KOH, 1.2 V window) outstripping

the performance of most commercial and lab-scale porous carbons from bioresources (50–100 F cm^{-3}, 1–3 W h L^{-1}, using 10 mg cm^{-2}). Even higher capacitances have also been achieved with spun lignin fibres (316 F g^{-1}, 1 A g^{-1}, 6 M KOH, 1 V window) although these were not free-standing electrodes.[234]

Park *et al.* took the concept of incorporating lignin into supercapacitors one step further by creating the electrolyte and electrode from lignin as shown in Fig. 5c.[217] The electrodes were formed from electrospun Alkali lignin/PAN solutions that were stabilized at 250 °C before being carbonized at 900 °C. The electrolyte was a flexible hydrogel, created by adding Alkali lignin (33% w/v) to 3.3 M KOH and 1.2 mmol l_{ignin} poly(ethylene glycol) digycidyl ether. This unique combination resulted in a flexible supercapacitor with a specific capacitance of 129.23 F g^{-1} (0.5 A g^{-1}, 1 V window), which was higher than when using a PVA/KOH gel electrolyte without lignin added (104.09 F g^{-1}). The increase in performance for the lignin hydrogel electrolyte was attributed to its higher conductivity than the PVA/KOH electrolyte.

The use of fossil derived polymers (*e.g.*, PAN, PEO, PVA,[235] PMMA, PVP) in lignin carbon fibres remains a large problem for their sustainability. Inspired by trees, Cao *et al.* investigated the covalent bonding of lignin to cellulose acetate to simulate the linkage between cellulose and lignin in trees to create carbon fibres. The lignin and cellulose acetate were covalently bonded to lignin by introducing epichlorohydrin as a connecting agent. The fibres were thermally stabilized (0.4 °C min^{-1}, 220 °C) and then carbonized at 600 °C under N_2. These fibres achieved a maximum SSA of 1061.7 m^2 g^{-1}, pore volume of 0.57 cm^3 g^{-1} and specific capacitance of 320.3 F g^{-1} (1 A g^{-1}, 6 M KOH, 1 V window). When 10% epichlorohydrin was used. Plant proteins can also be used to replace the fossil derived polymers. Yang *et al.* blended lignin with different hordein/zein ratios to create electrospun carbon fibres.[240] A ratio of 50/50 lignin to protein was found to be stable under carbonisation at 900 °C, forming a self-standing flexible carbon fibre mat that were subsequently activated with CO_2 at 850 °C. These fibres delivered a specific capacitance of 360 F g^{-1} (1 A g^{-1}, 6 M KOH, 1 V window). Interestingly, neither study used the carbon fibre mats as is, choosing to mix them with binders (polyvinylidene fluoride or polytetrafluoroethylene) and carbon black, suggesting that the electrode was not conductive enough or not stable as a free-standing mat. Regardless, these studies have demonstrated that it is possible to create carbon fibres without fossil fuel derived polymers and represent the next stage in green, renewable carbon fibres for supercapacitors. Table 3 summarizes the latest studies in the field of lignin-derived carbon materials for supercapacitors.

4. Lignin based thermoelectric materials

Generating electricity from low-grade waste heat (from sources below 100 °C) is a key enabler to reduce greenhouse gas emissions. Sources of low-grade heat (<100 °C) are ubiquitous in many industrial processes, electronics data centres and biological processes (metabolism). Significantly, 70% of all energy generated daily is lost as waste heat. Therefore, the conversion of waste heat into useful energy using the thermoelectric effect represents a huge opportunity to decrease carbon footprint of our society. Traditionally, inorganic compounds such as:

Table 3 Overview of lignin-derived carbon materials for supercapacitors

Electrolytes	Material	Specific surface area (m^2 g^{-1})	Cycling stability	Specific capacitance (F g^{-1})	Energy density (W h kg^{-1})	Ref.
6 M KOH	LHC-3K	1660	99% after 5000 cycles at 5 A g^{-1}	420 at 0.1 A g^{-1} 284 at 100 A g^{-1}	10 at 50 W kg^{-1}	189
6 M KOH	PLC-650-2	1069	93.5% after 10 000 cycles at 5 A g^{-1}	365 at 0.5 A g^{-1} 260 at 20 A g^{-1}	9.75 at 6157.9 W kg^{-1}	241
6 M KOH	3D-7-2K	1504	99.7% after 5000 cycles at 5 A g^{-1}	324 at 0.5 A g^{-1} 249 at 50 A g^{-1}	17.9 at 458 W kg^{-1}	242
6 M KOH and EMIM BF_4	L-700	1269	91.6% after 10 000 cycles at 5 A g^{-1}	300.5 at 0.5 A g^{-1}	8.5 at 100 W kg^{-1}	243
6 M KOH	NSC-700	1199	95.0% after 3000 cycles at 10 A g^{-1}	240.6 at 1 A g^{-1}	27.2 at 10 kW kg^{-1}	244
1 M H_2SO_4	3HPC/WO_3	1305	86.6% after 10 000 cycles at 10 A g^{-1}	432 at 0.5 A g^{-1} 214 at 20 A g^{-1}	34.3 at 237 W kg^{-1}	245
6 M KOH	AILCFN-3	736.14	84.7% after 3000 cycles 10 mA cm^{-2}	278.9 at 0.14 A g^{-1} 149.6 at 13.6 A g^{-1}	30.8 at 800 W kg^{-1}	246
6 M KOH	ARS/PGLS-1	1727.7	99.7% after 2000 cycles at 2 A g^{-1}	469.5 at 0.5 A g^{-1} 200.2 at 10.0 A g^{-1}	9.45 at 100.06 W kg^{-1}	247
PVA/H_2SO_4 gel	sLIG-O/S14	181.37	81.3% after 8000 cycles at 50 mV s^{-1}	53.2 mF cm^{-2} at 0.08 mA cm^{-2}	0.45 mW h cm^{-3} at 1.6 mW cm^{-2}	248
3.3 M KOH	ECNF	1176.0	99% after 10 000 cycles at 5 A g^{-1}	129.23 at 0.5 A g^{-1}	4.49 at 252 W kg^{-1}	217
6 M KOH	E-CNFs	2313	94.5% after 5000 cycles at 1 A g^{-1}	320 at 1 A g^{-1} 200.4 at 20 A g^{-1}	17.92 at 800 W kg^{-1}	249
1 M Na_2SO_4	LCNFs-MSSL-180-3 : 7	1254.5	90.6% at 10 A g^{-1}	533.7 at 0.5 A g^{-1}	69.7 at 780 W kg^{-1}	250
1 M H_2SO_4	LCNFs/PPy	872.60	77% after 1000 cycles at 4 A g^{-1}	213.7 at 1 A g^{-1}	—	251

Bi_2Te_3, PbTe and SiGe have dominated the manufacturing of energy harvesting devices. However, serious drawbacks such as: toxicity, scarcity of raw materials and high cost have limited their application and pushed research to newer alternative materials which are highly abundant, low cost and non-toxic. Thus, there is no current technology capable to satisfy the efficiency and sustainability requirements for low-grade heat conversion. A thermoelectric generator consists in n-type and p-type semiconductors that are connected electrically in series and thermally in parallel, when heat is apply through the thermoelectric junction a current flow is generated due to the Seebeck effect (voltage generated due to a thermal gradient). Thermoelectric efficiency is measured by the dimensionless figure of merit *ZT*:

$$ZT = \frac{S^2 \sigma T}{\kappa} \quad (1)$$

where *S*, *T*, σ and κ are the Seebeck coefficient, absolute temperature, electrical conductivity and thermal conductivity respectively. The power factor is calculated as follows:

$$\mathrm{PF} = S^2 \sigma \quad (2)$$

and is used to compare the thermoelectric efficiency of samples with similar thermal conductivities.[252–258]

Looking at this scenario, lignin has an enormous potential for a promising sustainable source to produce thermoelectric materials due to its ideal molecular structure to produce carbon nanostructures with semiconducting properties. This is an emerging field of application for lignin and there are not many studies published until now. One study published by the University of Limerick[259] showed enormous potential of lignin as precursor for carbon nanostructures with TE properties. Fig. 7 shows carbon nano fibres (CNFs) from lignin/PAN blends produced by electrospinning and their TE properties as a function of lignin content and processing conductions. The addition of lignin (up to 70%) reduces the diameter of CNFs from 450 nm to 250 nm, increases sample flexibility and promotes inter-fibre fusion. The results showed the possibility of a conversion of p-type to n-type semiconducting behaviour through doping with hydrazine vapour which allows the production of TEGs utilising both types of semiconductors based on lignin. CNFs depicted a maximum p-type power factor of 9.27 μW cm^{-1} K^{-2} for CNFs carbonised at 900 °C with 70% lignin which is a 34.5-fold increase to the CNFs with 0% lignin. For the hydrazine treated samples, the results showed a maximum n-type power factor of 10.2 μW cm^{-1} K^{-2} for the CNFs produced in the same way.

Other strategy to use lignin as part of thermoelectric materials is lignin can be used as dopant for carbon-based nanostructures due to its aromatic chemical structure that can tailor thermoelectric properties of multi-walled carbon nanotubes (MWCNTs).[260] This study shows how lignin can be valorised as a doping agent for TE devices resulting in outstanding performance levels outperforming fossil equivalents. The addition of lignin to Carbon Nanotube Yarns (CNTYs) improves their TE performance by one order of magnitude, showing for the first time that lignin can influence the transport properties of TE materials such as carbon nanotubes. In this case lignin increases electrical conductivity and Seebeck

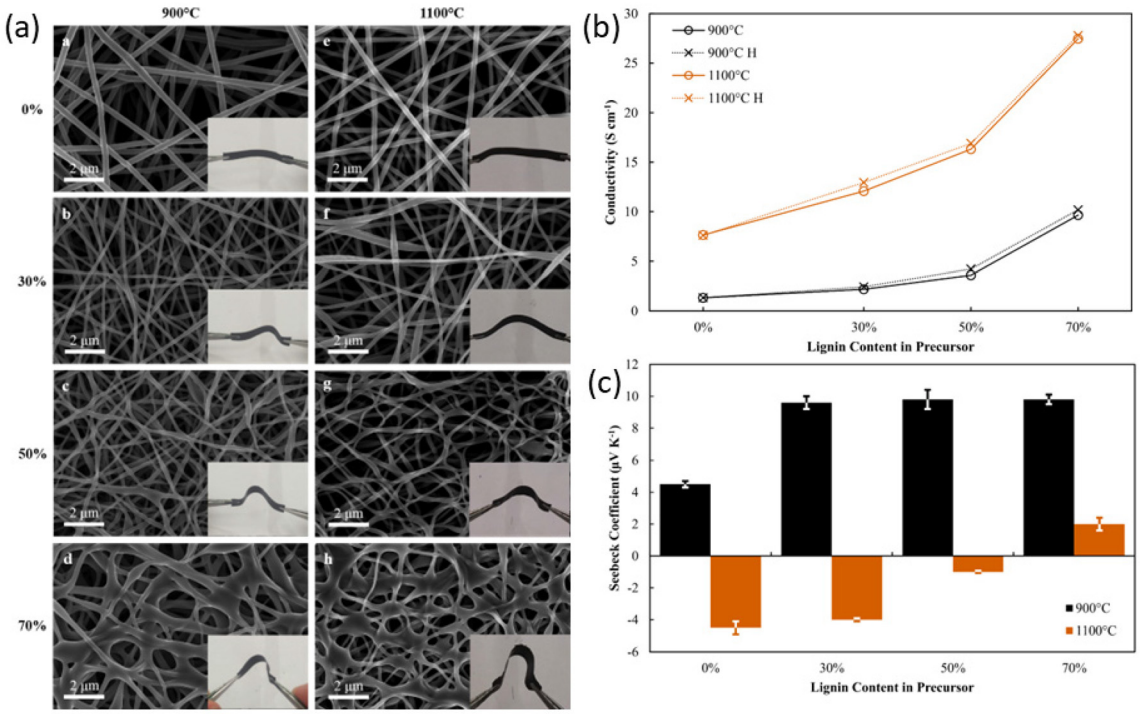

Fig. 7 (a) SEM images, (b) electrical conductivity and (c) Seebeck coefficient of lignin derived CNFs. Adapted with permission from ref. 256. Copyright 2019, Elsevier.

coefficients simultaneously (Fig. 8), which is considered the "Holy Grail" of TE materials. In addition, these materials show the possibility to manufacture TE generators with an outstanding power of 3.5 μW representing one of the highest values reported in literature for fully organic TE generators.

Another way to use lignin for thermal energy harvesting is the use of lignin as a photothermal material which can be combined with conventional TEGs to produce energy due to the temperature gradient generated due to light absorption of lignin.[261] This study demonstrated that lignin nanoparticles (L-NPs) can carry out photothermal conversion, which was attributed to π–π stacking of lignin molecules L-NPs showed a stable photothermal effect (22%). L-NPs were deposited on top of the TEGs as heat source generating around 0.12 V under irradiation of 100 mW cm^{-2}. Other studies have shown this strategy for photoresponsive actuator devices where lignin is blended with castor oil-derived polyamide elastomers to develop the photoactive part.[262]

This particular valorisation route has not many limitations in terms of lignin structure, morphology and source. In principle, the presence of hydroxyl groups in the vast majority of lignins, facilitates the functionalisation for a targeted doping in organic based thermoelectric materials. In addition, for the case of carbon-based semiconducting nanostructures derived from lignin, these hydroxyls groups can be used for crosslinking points to improve the carbon phase (better electric transport properties) generated by the aromatic ring condensation during the carbonisation process. Therefore, different types of lignin can be easily adapted to meet the requirements in the thermoelectric field.

5. Lignin for energy applications – biofuels

Finding alternative energy sources from renewable feedstocks is also a highly pursued objective. Lignin valorisation in this field is an interesting option due to its high energy density, related to its structure and the presence of aromatic units, outputting numerous patents (70 patents filed with the World Intellectual Property Organization for the last 3 years). Lignin

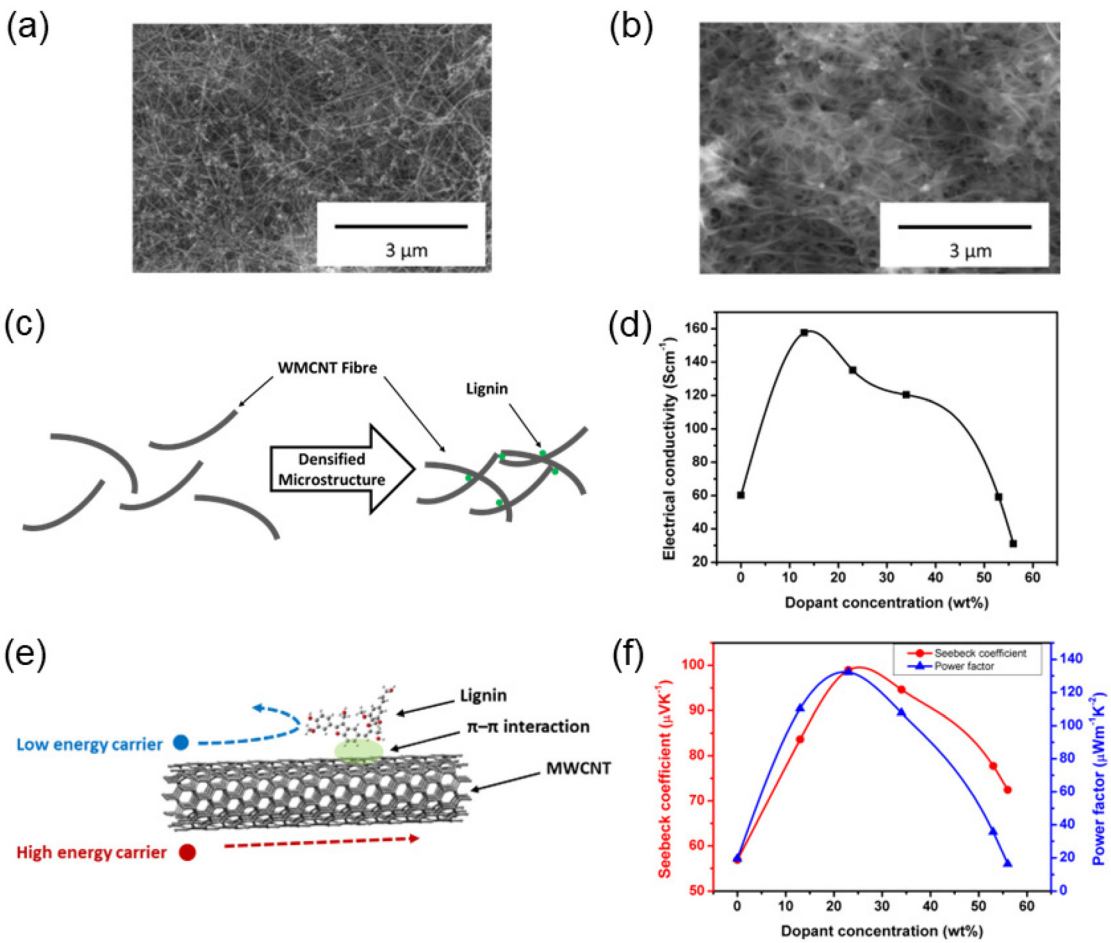

Fig. 8 SEM images of (a) pristine CNTY and (b) CNTY/lignin nanocomposite doped with 34 wt% lignin; schematic diagrams of (c) densified MWCNT fibre microstructure by incorporating lignin, (e) charge carrier filtering mechanism by introducing lignin; thermoelectric properties of CNTY/lignin nanocomposites with varying dopant levels: (d) electrical conductivity, (f) Seebeck coefficient and power factor. Adapted with permission from ref. 260. Copyright 2020, Wiley.

based biofuels could be classified as (i) solid lignin-derived chars (ii) liquid biofuels and (iii) hydrogen. Lignin conversion to fuels is mainly addressed either through depolymerization or gasification approaches. In particular, lignin derived liquid fuels could be accessed *via* depolymerization, hydrogenation and chemical upgrading steps. Besides, synthetic alcohols and Fischer–Tropsch liquid fuels could be obtained from syngas through gasification strategies.

Nowadays, most approaches for lignin utilisation are focused on its combustion, with a low energy efficiency. Hence, integrated schemes, involving depolymerisation towards aromatics and the further gasification of the remaining solids offer promising options which could potentially give rise to liquid, solid and gaseous fuels (Fig. 9). Several strategies have been developed to accomplish the catalytic hydrodeoxygenation of lignin and its derivatives, towards hydrocarbon (cyclohexanes and arenes depending on the catalytic approach) liquid fuels. Such hydrocarbons may also be catalytically transformed into syngas and hydrogen. For example, pure hydrogen may be obtained by conversion of syngas *via* water-shift reaction and subsequent gas separation.[263,264]

However, due to (i) the inherent complexity of the lignin structure with the presence of a wide distribution of bond types, including C–C and C–O of different strengths as mentioned earlier in this review, (ii) the heterogeneity of the lignin derived products from depolymerisation and (iii) the trend of the obtained low-weight compounds for recondensation reactions and catalysts poisoning, lignin conversion into fuels still represents a challenging research field.

A myriad of studies have been focused on the depolymerisation of lignin and further hydrodeoxygenation into hydrocarbons, passing by thermo-, photo-, electro and bio-catalytic routes, all of which consider lignin properties, reactivity and catalysts features.[263,265–268] Regarding bio-catalytic approaches, inspired by nature, enzymatic systems such as peroxidases and laccases has been investigated for lignin depolymerisation under mild conditions leading to the production of aromatics with low-molecular weight. Nonetheless, the employment of such biomimetic strategies also requires the reduction of the use of enzyme cofactors, whose price could affect the cost-efficiency of the overall process. Also, the natural recalcitrance of lignin hinders the efficiency of biomimetic degradation by providing an hydrophobic surface limiting the biotic and abiotic stresses.[269] Thermal strategies, through pyrolysis or its combination with hydrodeoxygenation catalysis towards fuels have also widely explored to overcome these challenges.

Even if not a trivial task, some recent studies have attempted to investigate the influence of lignin properties on the performance and quality of biofuels. For instance, Rodríguez-Soalleiro and co-workers have gotten insights into the influence of the physico-chemical features of lignin from different biomass wastes on the quality of biofuel pellets, noting that higher chlorine and ash contents have a detrimental effect not only on the heating value and energy performance but also on the environmental impact. Besides the relationship biomass composition-pellets quality, some correlations were also performed between the microstructure and distribution of lignin in the pellets and their efficiency.[270] The origin of the recalcitrance to enzymatic catalysis are believed to be partially linked to the S/G ratio of the biopolymer through carbon–carbon bonding between the lignin units.[269]

The design of efficient catalytic systems, considering metal entities and supports, has attained the attention of the scientific community, looking to overcome handicaps related to the material deactivation for coke formation or metal sintering. In this regard, transition metals have been widely investigated,

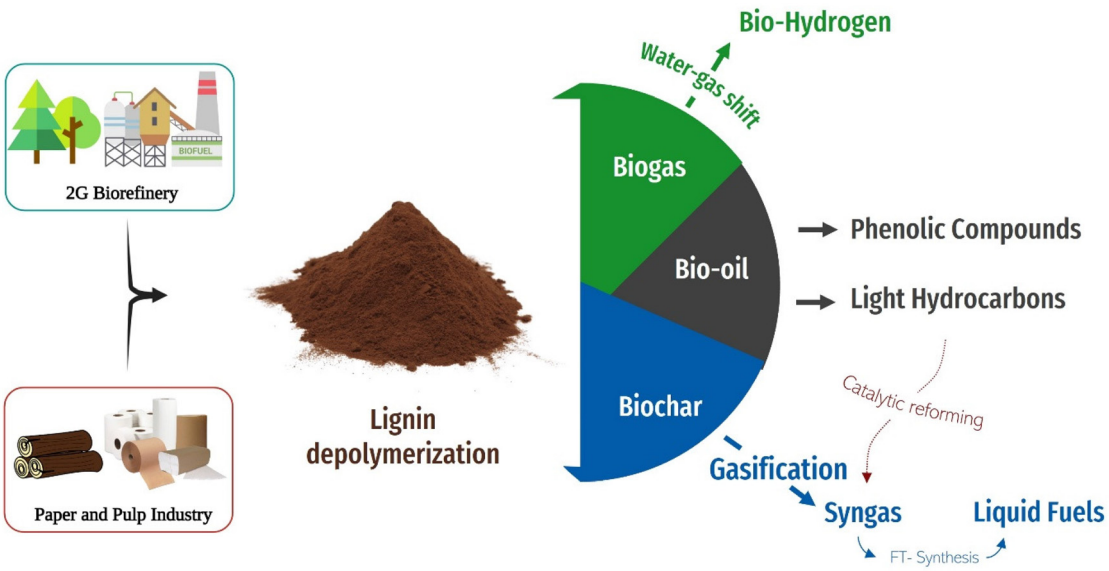

Fig. 9 Schematic representation of the processes involved in the upgrading of lignin to fuels.

either in one-pot or two-steps approaches involving lignin hydrogenolysis and hydrodeoxygenation reactions. For instance, lignin derived from corn wastes have been treated employing Ru nanoparticles supported over alumina and HY zeolite for the preparation of hydrocarbons, which could be employed as jet fuels. In particular, acid sites of HY zeolite played a crucial role on the depolymerisation of lignin *via* ether bond cleavage, while the Ru/Al_2O_3 catalyst promoted the HDO conversion into hydrocarbons. Following the aforementioned strategies, hydrocarbons were obtained with *ca.* 22% yield, from which alkylcyclohexanes represent a 90%.[271] Based on such results, a bifunctional catalyst was designed by supporting ruthenium nanoparticles on HY zeolite. Interestingly, the combination of noble metal nanoparticles and acid zeolite supports exhibited a synergistic effect on the HDO reaction of softwood derived lignin, leading to slightly higher yields of hydrocarbons (26–32 wt%).[272] Furthermore, similar catalytic systems, for instance based on Ru/Nb_2O_5 and Ru/Nb_2O_5 supported on silica, have been used for the hydrodeoxygenation reaction of birch-derived lignin for the production of hydrocarbons (C7–C9), achieving yields up to *ca.* 36% with high selectivity (71%) towards arene derivatives.[273] Besides the aforementioned ruthenium systems, Ni-based catalytic materials on silica/alumina supports have been also reported for the production of hydrocarbons (C3–C17) from cellulolytic enzyme lignin.[263] Moreover, bimetallic materials, based for instance on Ni–Mo or Co–Mo supported on alumina, have been used considering as well the needs to remove heteroatoms, such as sulphur and nitrogen. In this sense, the desired goal is to move toward non-noble metal-based materials to ensure the cost-efficiency of the protocol.

Furthermore, an interesting approach for lignin conversion into fuels has been recently proposed by mechanochemical methods, which could boost the sustainability of the process by decreasing the use of solvents and additional reagents, as well as reducing the required time.[274] In this regard, a wet milling oxidative strategy for lignin depolymerisation was proposed by Yao *et al.* employing KOH and toluene.[275] Such mechanochemical process was compared with the results of Baeyer–Villiger oxidation using porphyrin as catalytic specie, displaying improved results. Moreover, a synergistic effect was found by combining mechanochemistry and porphyrin oxidation strategies for lignin depolymersation.[276] In addition, solvent-less mechanochemical approaches have been also used for the oxidative cleavage of lignin or lignin β-O-4 model compounds with HO-TEMPO/KBr/oxone, leading to quinones and phenolic derivatives. Outstandingly, such strategy was translated to gram-scale, opening new possibilities for the industrial application of solvent-less mechanochemistry for lignin depolymerisation.[277]

Furthermore, mimicking photosynthesis process in nature, photocatalytic strategies for lignin conversion into fuels, through C–O and C–C cleavage,[278,279] is a promising possibility to move towards more environmentally friendly and economically efficient approaches, especially considering the possibility to use sun-type light irradiation.[280–283] Indeed, β-O-4 cleavage in lignin could be attempted through photocatalytic reductive (initiated by electrons or reducing agents), oxidative (initiated by holes or oxidant agents) or redox neutral (initiated by hole or oxidative species, together with electrons) routes, employing metal oxides, metal sulfides, quantum dots (QDs), organometallic complexes and carbon-based materials such as graphitic carbonitride.[284,285]

In addition, electrocatalytic and photo-assisted electrocatalytic routes have been investigated for the degradation of lignin for instance *via* lignin-enhanced water electrolysis or for the production of hydrogen. Regarding water electrolysis, the oxidation of lignin, among other molecules or even the direct use of biomass wastes, has been investigated as an economically feasible option to replace anodic oxidation, leading also to the generation of hydrogen at low potentials. As well, electrocatalysis have been employed for the conversion of lignin into valuable chemicals (such as vanillin, phenol and guaiacol) and fuels.[286]

Environmental and economic viability of lignin transformation into fuels is also an area which requires a lot of attention in order to ensure the competitiveness of such biorefinery scheme. In this direction, some studies have been performed by Life Cycle Assessment (LCA) analysis of the pyrolytic transformation of lignin into two types of biofuels depending on the sulphur content.[287]

6. Environmental and cost impact of lignin-based materials and products

The environmental and economic impact of the production of lignin can be quantified using tools such as life cycle assessment (LCA) and techno-economic analysis (TEA). The implementation of an LCA is governed by the ISO 14040-2006 and 14044-2006.[288] This assessment takes in consideration a product's life cycle in full (cradle-to-grave) or to its intended primary user (cradle-to-gate) to evaluate its environmental impact. Various factors are modelled, such as global warming potential (GWP, in $CO_{2,eq.}$ per kg of product); acidification (in $H_2SO_{4,eq.}$ per kg of product), Human Toxicity; ozone depletion *etc*. An LCA is typically conducted in four phases, the goal and scope definition phase; the inventory analysis phase; the impact assessment phase and the interpretation phase. It is widely used to estimate the environmental impact or benefit of an existing or new technology. Since the interest on lignin as an alternative to fossil-fuels based technologies has gained considerable attention recently, lignin-only LCA studies have emerged, which are either focused on lignin extraction[289–299] or lignin-based products (asphalt,[300–304] adhesives,[305–307] resins,[308] fine chemicals,[309–311,312–314] carbon fibres[315] and fuels.[287,316–320] Lignin as a product from biorefineries is a new concept, therefore most of the LCA conducted are based on either well quantified extraction processes such as Kraft or based on experimental lab scale data which has been extrapolated. In the latest case, the LCA allows to evaluate the environmental impact of an upscaled biorefinery.[292] Ran in parallel to

an LCA, a TEA includes process design, simulation, calculation of capital and operating cost along with installation cost of equipment for commercial scaled biorefinery.[321] The output of a TEA is minimal selling price (MSP), revenue and profitability. They are expressed in a similar functional unit as the LCA results. Here we focus on the LCA and TEA performed on lignin processes and materials relevant to energy applications.

6.1. Challenges encountered carrying out LCA on lignin

While a very useful tool to quantify the environmental impact of a product life cycle, LCA has its limitations,[322] which appear at all level of the process. LCA where lignin is the end product typically uses 1 kg lignin as the functional unit.[299,300,323] The country where the product is manufactured affects the outcome of an LCA. For example, the carbon footprint of electricity is significantly lower where renewable or nuclear energy sources are used. The impact on lignin production is illustrated in ref. 292 where the lignin produced in Sweden has a global warming potential GWP three times lower than that of a global lignin (1.68 *vs.* 5.5 $kgCO_{2,eq.}$ per kg lignin). The lifetime of the product affects how the LCA is conducted. Lignin is a wood-based product. Due to the CO_2 sequestration potential of wood, the definition of the system boundaries can be shifted.[324,325] It takes between 20 and 80 years for softwood trees to absorb its equivalent in CO_2.[321] Therefore, most LCA's are conducted over a period of 100 years to assume carbon neutrality.[324] While plausible when looking at lignin-based products for buildings, this assumption becomes problematic for carbon materials from lignin. A battery pack has a lifetime of 2–5 years. Incineration at the end of life would provoke a release of CO_2 unaccounted for in the LCA. Therefore, a wood-based product with a lifetime less than 100 years would need to account on the amount of $CO_{2,eq.}$ released by the incineration of the wood used in the product manufacture (between 1.95 to 2.08 $CO_{2\ eq.,kg}$ per kg of wood, dependant on the plant species and age[325]).

The lignin-only LCA studies are notoriously difficult to conduct, as well outlined by Moretti *et al.*[324] At the inventory phase, the approximation made on the data used (upscale simulated data based on lab scale processes,[292,293,299] secondary data from literature[301]) can impact the results. Most recent LCA conducted on lignin use data provided by biorefineries, leading to more reliable results.[300] Due to the nature of a biorefinery, lignin is the product of a multi-output process:[323] the allocation of the environmental impact between lignin and its co-products (such as cellulose, electricity, ethanol) from biorefineries is of most importance to quantify the GWP.[300,316,326,327] The ISO 14044:2006 guidelines provides a hierarchy to deal with multi-product systems such as biorefineries, with three levels: subdivision, system expansion and allocation.[288] This subdivision system, which uses data with higher level of details, is rendered difficult by the integration of the biorefinery systems.[323,324] System expansion modifies the system boundaries to include all the production of all functions. For a biorefinery, this means quantifying the impact of the whole process and not lignin extraction alone.[288,294,296] The allocation method uses physical parameters (mass, energy, economic values, *etc.*) to measure the impact of a product. For example, if a biorefinery outputs 100 kg of product, including 41 kg of lignin, lignin will be allocated 41% of the GWP. This method is used by close to a third of the LCA published before 2021.[324] However, it doesn't allocate an impact to heat or electricity, which are mass-free.[323] Similarly, energy allocation (13% of the studies[324]) uses energy value to allocate the GWP, which excluded CO_2. Economic allocation (16% of the studies[324]) uses the value of one product to evaluate its GWP. As lignin is typically a by-product, its value is low (0.3 euro per kg), leading to a low GWP by economic allocation. While its value has been low, it could increase due to the overall energy cost increase, therefore increasing lignin environmental impact. Obydenkova *et al.* allocated the environmental impacts between the three products of a lignocellulosic biorefinery producing ethanol, lignin oligomers and electricity using a subdivision matrix approach. Depending on the allocation method, they quantified the GWP of the lignin oligomers between 6.8 and 31.6 $kgCO_{2\text{-}eq.}$ per GJ.[328] Hermansen *et al.* ran different allocation scenarios on the lignin produced from a Kraft mill. The results varied between 0.18 to 0.64 kg $CO_{2\ eq.}$ per kg lignin. As mentioned before, the disparity between the functional units renders results difficult to compare. While LCA is a powerful tool, its completion necessitates a well-defined methodology and clearly stated assumptions.[324]

6.2. LCA of lignin and lignin-based products

The kraft process has been investigated for LCA in several studies.[289,299,301,323,329] Bernier focuses on how the extraction of lignin from black liquor positively impacts the overall production output by de-bottlenecking the recovery boiler. He also considers the carbon sequestration from the feedstock, almost cancelling the on-site carbon emissions.[299] These assumptions allow for a GWP of 0.57 kg $CO_{2,eq.}$ per kg lignin. However, they assume that the lignin produced has a 100 years lifetime. It is to be noted that the Bernier study is used as secondary data in subsequent articles. Another reference study from Culbertson estimated GWP of a softwood kraft pulp mill between 0.55–0.60 kg $CO_{2,eq.}$ per kg lignin. The de-bottlenecking of the recovery boiler allowed for a 5% increase in the efficiency of the pulp extraction process. As an environmental impact, the acidification was not systematically evaluated. Moretti's studies on Asphalt produced from Kraft mills assigned between 7 to 10% of the whole environmental impact to acidification (*vs.* 20 to 54% to GWP).[300,301] According to Culbertson, between 58%–68% of the acidification is due to the use of natural gas. Bernier evaluated the acidification value to be 5.3×10^{-3} kg $SO_{2,eq.}$ per kg Kraft lignin, due to the H_2SO_4 wash of the black liquor.[299]

The impact of the organosolv process was estimated in ref. 293, 329 and 330. Arias *et al.*[329] estimated the impact of the organosolv process twice as high as that of the Kraft process during the production of a bioadhesive. However, two pathways are taken in consideration for the lignin chemical modifi-

cation and bio-adhesive production, rendering the comparison between kraft and Organosolv GWP difficult. Yadav *et al.*[330] compared the organosolv process on a spruce bark using ethanol or bio-ethanol, at lab scale. The bio-ethanol process has a GWP of 1.54 kg $CO_{2,eq.}$ per kg lignin against 2.24 kg $CO_{2,eq.}$ per kg lignin for ethanol. The ethanol and the electricity have the highest impacts on the production (respectively 55% and 30%). The cost of production was estimated between €1.38–2.2 per kg lignin.

Teh *et al.*[295] compared the impact between alkali and organosolv process for the formation of nanoparticles of lignin from birch chip wood. The study uses extrapolated upscale data from lab scale. The alkali process has an impact 4–5 times lower than that of the organosolv treatment. The authors assigned this significant increase to the use of electricity. No TEA was performed.

The lignin-rich oil obtained from reductive catalytic fractionation was accounted for 57% of a biorefinery capital costs, with a MSP of 1.12 USD per kg and a GWP of 0.079 kg $CO_{2,eq.}$ per kg. In this study, the carbon sink of the growing feedstock (hybrid poplar) is accounted for, which offsets the overall GWP of the lignin fraction close to neutral.[297] No TEA was performed.

DES pretreatment (choline chloride – oxalic acid dihydrate) to form lignin-containing nanocellulose has an impact that is 2.5 times that of Sulfuric acid hydrolysis. The largest contribution was from the DES chemicals, between 52–63% for GWP.[291]

Kulas *et al.*[290] recently ran an LCA on kraft lignin as a product of a modified black liquor process. The data used was extrapolated from the lab scale work published and patented by Thies *et al.*[290] In this process, ethanol at 115 °C and 6.2 bar allow for a liquid–liquid solvent recovery from black liquor. The lignin solution is then dried off to recover lignin. The low boiling point of ethanol (78.4 °C) reduces the energy consumption of ethanol. The GWP of the lignin was evaluated at 4.0 kg $CO_{2,eq.}$ per kg lignin, assuming carbon neutrality from lignin. The MSP was estimated at 0.45 USD per kg lignin, cheaper than carbon fibre precursor PAN (2 USD per kg). Furthermore, Kulas performed an LCA on potential production of carbon fibres and activated carbon using an allocation by both mass and economical values, obtained from literature. The GWP of lignin-based carbon fibres was estimated at 20–22 kg $CO_{2,eq.}$ per kg of CF and the activated carbon at 5–12 kg $CO_{2,eq.}$ per kg. The cost of a kg of carbon fibre was estimated at USD 21.78 (depending on grade with higher grades much more expensive), generating a profit of USD 9.76 per kg. For a production based on a production of 6260 tonnes of CF per year for the US, the profit made is of USD 61 million yearly.

The LCA ran for biofuels are different in the terms of product lifetime, usually very short (days-months). The carbon neutrality assumption cannot be made. The studies all refer to the U.S. renewable fuel standard (RFS) which sets a 60% reduction on the greenhouse gas emissions (76% CO_2, 16% methane, 6% nitrous oxide, HFC) for cellulosic biofuels.[331] The results vary whereas the biorefinery produces its own electricity or not.[287] The functional unit is of 1 MJ. Obydenkova uses cornstover as feedstock to an ethanol–lignin biorefinery, from lab scale data. The lignin-derived automotive fuel minimal cost is between 14.4–18.1 USD per GJ, where the cheapest fuel is produced using natural gas as the energy source. The GHG emission targets are only met for lignin-derived automotive fuel for a biorefinery when all the impact is allocated to ethanol production.[287] Bartling *et al.* identified 12 biofuels that reaches the GHG emission targets. However, lignin is considered only as energy cogeneration in this study.[320] The LCA on bio-jet fuel from poplar biomass was performed by Budsberg *et al.*[318] This study uses lignin as a source of H_2 using hog fuel as the alternative energy source.

The pursuit of LCA for the production and use of lignin shows that lignin is a suitable alternative to fossil sources. It is clear that, when it comes to lignin and its products, LCA data should be analysed with a degree of caution as the methodologies employed have a strong impact on results. Also, current literature lacks assessments carried out on energy applications, outside of the biofuel field. This is mainly due to the emergence of this field and therefore the lack of available data. There is an obvious gap here for future studies.

7. Outlook

Lignin extraction necessitates non-destructive, upscalable extraction processes that preserve the ether bonds and phenolic groups. The emergence of economically viable biorefineries is a welcome step for the use of lignin for energy applications. However many stumbling blocks remain, for example, the depolymerisation processes for the production of biofuels are yet to be fully upscaled. For batteries improvements in performance of lignin-based electrodes in full cell batteries should be the ultimate ambition.

For energy storage in general (batteries and supercapacitors), optimisation of electrode architecture is extremely important for maximized electrochemical performance with emerging emphasis on interconnected pore networks, surface area, lignin CNF design features (diameter, length and network rigidity), density/areal loading, and the adoption of cost effective production strategies suitable for scalability such as 3D patterning technologies. These designs need to allow for electrode swelling particularly when combined with high-capacity Li alloying materials like Si which is hugely affected by volumetric expansion (Si > 300%), leading to a long term cycling capacity drop, reduced rate capability, and increased safety concerns. Such issues should be addressed at the capacity enhancing material level (*e.g.*, Si, In, oxides, *etc.*) by adopting design strategies that will prevent segregation, pulverisation, and cracking. At the electrode level a balanced distribution of voids/pores, network rigidity, and density of active elements must be judiciously controlled to regulate swelling and capacity fading during long term cycling. However, this may require a reasonable trade-off between the electrode features, such as robust structures, energy density/capacity, side

reactions, and full cell performance. Consequently, a rational design of composite or more complex electrodes could offer more choices for enhancing the performance of lignin-based electrodes that may become suitable for practical batteries.

To practically deploy lignin electrodes in high-energy density batteries, it is also crucial to investigate the electrochemical behaviour relative to the electrode structure, including the swelling characteristics both in half-cell and full-cell configurations, but this is currently lacking in the literature. The specific impact of non-lignin containing cell components such as conventional electrolytes, binders, and conductive additives on the performance of the lignin-derived electrodes is rarely investigated and should be a focus of future research. We believe that a comprehensive design of lignin-based cells with the specific goal of achieving high energy density, based on high capacity lignin-derived composite anode/cathodes will lay a strong foundation toward the realization of higher-energy batteries than graphite. Despite the significant research progress in developing lignin-based anodes and cathodes, it is still not exactly clear how the specific type of lignin and their functionalized structures or carbonization processes impact the final anode features and performance of various battery types besides the porosity and CNF networking features commonly observed. Therefore, advanced nanoscale characterization techniques for detailed study and in-depth understanding of the structure–property relationship are required to reliably determine the electrochemical mechanisms, particularly for composite structures (*e.g.*, carbon/Si anodes). Operando characterization, *in situ* studies, and theoretical analysis are also strongly recommended for detailed studies and in-depth understanding of the behaviour of lignin based cell components with respect to ion transport and structural behaviour during the charge/discharge processes. The culmination of these studies could reliably predict and provide clearer understanding of the dynamic electrode kinetics during cycling, thereby providing a better understanding of the redox chemistry, failure dynamics, and the charge storage mechanisms, thus, clearing the path to allow for the efficient design and development of lignin-based materials in practical batteries.

While promising, the valorisation of lignin into a sustainable and economical biofuel necessitates fully developed depolymerisation pathways. The complexity of the lignin structure and its natural recalcitrance to degradation limits the effectiveness of the depolymerisation process. The variety of aromatics outputted from the depolymerisation triggers need for complex separation processes. Thermoelectric future directions will focus on how to develop hybrid carbon-based nanostructures derived from lignin in combination with other inorganic materials to improve their thermoelectric performance. While this field is still very much in its infancy the emerging potential is clear to see.

In terms of LCA and technoeconomic analysis while lignin is typically abundant and a low-cost material (often considered waste), future study on the development and deployment of lignin electrodes in energy storage devices should include practical cost benefits analysis particularly the energy-to-price ratio. While most researchers heavily emphasized its cost and environmental benefits, the combined processing/treatment and transformation steps of pristine lignin into an active carbon electrode material and integration of secondary materials could be relatively costly. Moreover, the use of chemical activation processes and combination with toxic polymeric materials (also requiring further process steps) make the environmental benignity of the electrode materials and "green battery" claims debatable. Also, by blending lignin with such polymer materials in the various cell components (anode, cathode, electrolyte, binder and separator), it is misleading as commonly captured in most literatures to refer to the final composite material as a lignin derivative as the secondary materials do not contain lignin.

8. Concluding remarks

Lignin is a unique polymer within biomass. It presents a one of a kind aromatic structure and a high carbon content. Above all, its production does not compete with food supply chains and its valorisation allows for use of an ever increasing amount of waste. As a result of the active interest of research bodies and industries into candidates to replace oil-based materials, lignin is being extensively investigated for use in functional materials. In particular, the development of lignin-based materials for energy applications has shown enormous promise. Lignin is finding application in a remarkable array of different battery components including electrode materials, separators and electrolytes. Research into lignin-derived carbon materials, especially hard carbons, is rapidly gaining interest in particular for applications beyond lithium ion where larger ions can be accommodated by intercalation between graphitic layers where lignin derived carbons outperform conventional graphite anodes. Clearly, exploitation of lignin as a material for components has enormous potential to lower overall battery cost and contribute to the development of safer and more sustainable energy storage devices. Control of the unique porous carbon architectures derived from lignin also offers advantages in supercapacitors and thermoelectric devices where lignin derived materials have produced devices with beyond state of the art seebeck coefficients and power factors. In particular, for the thermoelectric field, lignin could have an enormous potential not only as carbon precursors for electronic semiconductors but also as platform for ionic thermoelectric materials which have recently emerged as a plausible alternative to classical thermoelectric devices.

However, progress in all these applications can only be sustained by the continuous supply of a high-quality lignin, as its properties are strongly dependent on source and extraction method. This calls for the development of versatile processing routes and the provision of industrial scale biorefineries, to possibly produce predefined lignin chemical structures with the aid of artificial intelligence and machine learning. This

may help in the elucidation of structure/property/function relationships of lignin precursors and the tailoring of their carbonised products for next generation energy applications.

Conflicts of interest

There are no conflicts to declare.

Acknowledgements

This research was supported by Irish Government funding *via* the DAFM NXTGENWOOD research program 2019PROG704. This work also received support from the Science Foundation Ireland (SFI) (contract no. 11-PI-1148, 16/IA/4629 and SFI 16/M-ERA/3419) and the European Union's Horizon 2020 Research and Innovation Program; grant agreement no. 814464 (Si-DRIVE project). T. K. acknowledges support from the Sustainable Energy Authority of Ireland through the Research Development and Demonstration Funding Programme (grant no. 19/RDD/548) and Enterprise Ireland through the Innovation Partnership Programme (grant no. IP 2019 0910). I. S. A. acknowledges support from the SFI Industry RD&I Fellowship Programme (21/IRDIF/9876) and the EU Horizon 2020 research and innovation program under the Marie Sklodowska-Curie Individual Fellowship Grant (843621). A. B. and M. N. C. acknowleges support from VIBES which has received funding from the Biobased Industries Joint Undertaking (JU) under the European Union's Horizon 2020 research and innovation programme under grant agreement No 101023190. The JU receives support from the European Union's Horizon 2020 research and innovation programme and the Bio-based Industries Consortium.

References

1 T. Kobayashi and L. Nakajima, *Curr. Opin. Green Sustain. Chem.*, 2021, **28**, 100439.
2 M. Muddasar, R. Liaquat, A. Aslam, M. Z. Ur Rahman, A. Abdullah, A. H. Khoja, K. Latif and A. Bahadar, *Int. J. Energy Res.*, 2022, 5625–5645.
3 T. Hák, S. Janoušková and B. Moldan, *Ecol. Indic.*, 2016, **60**, 565–573.
4 E. E. Miller, Y. Hua and F. H. Tezel, *J. Energy Storage*, 2018, **20**, 30–40.
5 S. Iqbal, H. Khatoon, A. Hussain Pandit and S. Ahmad, *Mater. Sci. Energy Technol.*, 2019, **2**, 417–428.
6 L. Wang and X. Hu, *Chem. – Asian J.*, 2018, **13**, 1518–1529.
7 M. I. Din, S. Ashraf and A. Intisar, *Sci. Prog.*, 2017, **100**, 299–312.
8 T. Yoda, K. Shibuya and H. Myoubudani, *Measurement*, 2018, **125**, 572–576.
9 S. Li, W. Li and Z. Fan, *Biomass Based Energy Storage Mater.*, 2020, **78**, 124–142.
10 W. Zhang, J. Yin, C. Wang, L. Zhao, W. Jian, K. Lu, H. Lin, X. Qiu and H. N. Alshareef, *Small Methods*, 2021, **5**, 2100896.
11 X. Wu, J. Jiang, C. Wang, J. Liu, Y. Pu, A. Ragauskas, S. Li and B. Yang, *Biofuels, Bioprod. Biorefin.*, 2020, **14**, 650–672.
12 W. Boerjan, J. Ralph and M. Baucher, *Annu. Rev. Plant Biol.*, 2003, **54**, 519–546.
13 J. C. Carvajal, Á. Gómez and C. A. Cardona, *Bioresour. Technol.*, 2016, **214**, 468–476.
14 D. Di Francesco, C. Dahlstrand, J. Löfstedt, A. Orebom, J. Verendel, C. Carrick, Å. Håkansson, S. Eriksson, H. Rådberg, H. Wallmo, M. Wimby, F. Huber, C. Federsel, M. Backmark and J. S. M. Samec, *ChemSusChem*, 2021, **14**, 2414–2425.
15 J. A. Poveda-Giraldo, J. C. Solarte-Toro and C. A. Cardona Alzate, *Renewable Sustainable Energy Rev.*, 2021, **138**, 110688.
16 P. Jędrzejczak, M. N. Collins, T. Jesionowski and Ł. Klapiszewski, *Int. J. Biol. Macromol.*, 2021, **187**, 624–650.
17 J. Sternberg, O. Sequerth and S. Pilla, *Prog. Polym. Sci.*, 2021, **113**, 101344.
18 E. Lizundia, M. H. Sipponen, L. G. Greca, M. Balakshin, B. L. Tardy, O. J. Rojas and D. Puglia, *Green Chem.*, 2021, **23**, 6698–6760.
19 H. Hatakeyama and T. Hatakeyama, in *Biopolymers*, 2009, ch. 12, pp. 1–63, DOI: 10.1007/12_2009_12.
20 S. Sen, S. Patil and D. S. Argyropoulos, *Green Chem.*, 2015, **17**, 4862–4887.
21 K. Lundquist and J. Parkås, *BioResources*, 2011, **6**, 920–926.
22 Y. Lu, Y.-C. Lu, H.-Q. Hu, F.-J. Xie, X.-Y. Wei and X. Fan, *J. Spectrosc.*, 2017, **2017**, 8951658.
23 R. Rinaldi, R. Jastrzebski, M. T. Clough, J. Ralph, M. Kennema, P. C. A. Bruijnincx and B. M. Weckhuysen, *Angew. Chem., Int. Ed.*, 2016, **55**, 8164–8215.
24 F. G. Calvo-Flores, J. A. Dobado, J. Isac-García and F. J. Martín-Martínez, *Lignin and lignans as renewable raw materials: chemistry, technology and applications*, John Wiley & Sons, 2015.
25 A. Duval and M. Lawoko, *React. Funct. Polym.*, 2014, **85**, 78–96.
26 Y. Mottiar, R. Vanholme, W. Boerjan, J. Ralph and S. D. Mansfield, *Curr. Opin. Biotechnol.*, 2016, **37**, 190–200.
27 T. Z. H. Gani, M. J. Orella, E. M. Anderson, M. L. Stone, F. R. Brushett, G. T. Beckham and Y. Román-Leshkov, *ACS Sustainable Chem. Eng.*, 2019, **7**, 13270–13277.
28 W. Fang, S. Yang, X.-L. Wang, T.-Q. Yuan and R.-C. Sun, *Green Chem.*, 2017, **19**, 1794–1827.
29 D. S. Bajwa, G. Pourhashem, A. H. Ullah and S. G. Bajwa, *Ind. Crops Prod.*, 2019, **139**, 111526.
30 L. Dessbesell, M. Paleologou, M. Leitch, R. Pulkki and C. Xu, *Renewable Sustainable Energy Rev.*, 2020, **123**, 109768.
31 T. Li and S. Takkellapati, *Biofuels, Bioprod. Biorefin.*, 2018, **12**, 756–787.
32 A. G. Vishtal and A. Kraslawski, *BioResources*, 2011, **6**, 3547–3568.

33 T. Aro and P. Fatehi, *ChemSusChem*, 2017, **10**, 1861–1877.
34 K. Lundquist, R. Simonson and K. Tingsvik, *Sven. Papperstidn.*, 1983, **86**, 44–47.
35 S. Constant, H. L. J. Wienk, A. E. Frissen, P. D. Peinder, R. Boelens, D. S. van Es, R. J. H. Grisel, B. M. Weckhuysen, W. J. J. Huijgen, R. J. A. Gosselink and P. C. A. Bruijnincx, *Green Chem.*, 2016, **18**, 2651–2665.
36 M. A. Karnofski, *J. Chem. Educ.*, 1975, **52**, 490.
37 D. S. Bajwa, G. Pourhashem, A. H. Ullah and S. G. Bajwa, *Ind. Crops Prod.*, 2019, **139**, 111526.
38 S. Y. Lin and I. S. Lin, *Ullmann's encyclopedia of industrial chemistry*, Verlag Chemie, Hoboken, NJ, 1991.
39 A. BjÖRkman, *Nature*, 1954, **174**, 1057–1058.
40 J.-L. Wen, B.-L. Xue, F. Xu, R.-C. Sun and A. Pinkert, *Ind. Crops Prod.*, 2013, **42**, 332–343.
41 J. Rencoret, G. Marques, A. Gutiérrez, L. Nieto, J. I. Santos, J. Jiménez-Barbero, Á. T. Martínez and J. C. del Río, *Wood Research and Technology*, 2009, **63**, 691–698.
42 M.-F. Li, S.-N. Sun, F. Xu and R.-C. Sun, *Chem. Eng. J.*, 2012, **179**, 80–89.
43 H. Wang, Z. Liu, L. Hui, L. Ma, X. Zheng, J. Li and Y. Zhang, *Holzforschung*, 2020, **74**, 275–285.
44 C. Huang, X. Jiang, X. Shen, J. Hu, W. Tang, X. Wu, A. Ragauskas, H. Jameel, X. Meng and Q. Yong, *Renewable Sustainable Energy Rev.*, 2022, **154**, 111822.
45 D. Dondi, A. Zeffiro, A. Speltini, C. Tomasi, D. Vadivel and A. Buttafava, *J. Anal. Appl. Pyrolysis*, 2014, **107**, 53–58.
46 T. Han, N. Sophonrat, P. Evangelopoulos, H. Persson, W. Yang and P. Jönsson, *J. Anal. Appl. Pyrolysis*, 2018, **133**, 162–168.
47 V. Ashokkumar, R. Venkatkarthick, S. Jayashree, S. Chuetor, S. Dharmaraj, G. Kumar, W.-H. Chen and C. Ngamcharussrivichai, *Bioresour. Technol.*, 2022, **344**, 126195.
48 S. Hong, X.-J. Shen, Z. Xue, Z. Sun and T.-Q. Yuan, *Green Chem.*, 2020, **22**, 7219–7232.
49 Y. T. Tan, A. S. M. Chua and G. C. Ngoh, *Bioresour. Technol.*, 2020, **297**, 122522.
50 W. Wang and D.-J. Lee, *Bioresour. Technol.*, 2021, **339**, 125587.
51 Y. Wang, K. H. Kim, K. Jeong, N.-K. Kim and C. G. Yoo, *Curr. Opin. Green Sustain. Chem.*, 2021, **27**, 100396.
52 A. P. Abbott, G. Capper, D. L. Davies, R. K. Rasheed and V. Tambyrajah, *Chem. Commun.*, 2003, 70–71, DOI: **10.1039/B210714G**.
53 C. R. Ashworth, R. P. Matthews, T. Welton and P. A. Hunt, *Phys. Chem. Chem. Phys.*, 2016, **18**, 18145–18160.
54 O. S. Hammond, D. T. Bowron and K. J. Edler, *Green Chem.*, 2016, **18**, 2736–2744.
55 C. F. Araujo, J. A. P. Coutinho, M. M. Nolasco, S. F. Parker, P. J. A. Ribeiro-Claro, S. Rudić, B. I. G. Soares and P. D. Vaz, *Phys. Chem. Chem. Phys.*, 2017, **19**, 17998–18009.
56 E. Posada, M. J. Roldán-Ruiz, R. J. Jiménez Riobóo, M. C. Gutiérrez, M. L. Ferrer and F. del Monte, *J. Mol. Liq.*, 2019, **276**, 196–203.
57 E. Posada, N. López-Salas, D. Carriazo, M. A. Muñoz-Márquez, C. O. Ania, R. J. Jiménez-Riobóo, M. C. Gutiérrez, M. L. Ferrer and F. D. Monte, *Carbon*, 2017, **123**, 536–547.
58 Y. Bai, X.-F. Zhang, Z. Wang, T. Zheng and J. Yao, *Bioresour. Technol.*, 2022, **347**, 126723.
59 V. Provost, S. Dumarcay, I. Ziegler-Devin, M. Boltoeva, D. Trébouet and M. Villain-Gambier, *Bioresour. Technol.*, 2022, **349**, 126837.
60 Y. T. Tan, G. C. Ngoh and A. S. M. Chua, *Bioresour. Technol.*, 2019, **281**, 359–366.
61 C.-W. Zhang, S.-Q. Xia and P.-S. Ma, *Bioresour. Technol.*, 2016, **219**, 1–5.
62 Q. Xia, Y. Liu, J. Meng, W. Cheng, W. Chen, S. Liu, Y. Liu, J. Li and H. Yu, *Green Chem.*, 2018, **20**, 2711–2721.
63 Y. Liu, W. Chen, Q. Xia, B. Guo, Q. Wang, S. Liu, Y. Liu, J. Li and H. Yu, *ChemSusChem*, 2017, **10**, 1692–1700.
64 A. M. da Costa Lopes, J. R. B. Gomes, J. A. P. Coutinho and A. J. D. Silvestre, *Green Chem.*, 2020, **22**, 2474–2487.
65 Z. Chen, X. Bai and A. Lusi, *ACS Sustainable Chem. Eng.*, 2018, **6**, 12205–12216.
66 Z. Chen, W. D. Reznicek and C. Wan, *Bioresour. Technol.*, 2018, **263**, 40–48.
67 Z. Chen, X. Bai, A. Lusi and C. Wan, *ACS Sustainable Chem. Eng.*, 2020, **8**, 9783–9793.
68 B. Soares, A. M. da Costa Lopes, A. J. D. Silvestre, P. C. Rodrigues Pinto, C. S. R. Freire and J. A. P. Coutinho, *Ind. Crops Prod.*, 2021, **160**, 113128.
69 M. C. Gutiérrez, M. L. Ferrer, C. R. Mateo and F. del Monte, *Langmuir*, 2009, **25**, 5509–5515.
70 N. López-Salas, J. M. Vicent-Luna, S. Imberti, E. Posada, M. J. Roldán, J. A. Anta, S. R. G. Balestra, R. M. Madero Castro, S. Calero, R. J. Jiménez-Riobóo, M. C. Gutiérrez, M. L. Ferrer and F. del Monte, *ACS Sustainable Chem. Eng.*, 2019, **7**, 17565–17573.
71 N. López-Salas, J. M. Vicent-Luna, E. Posada, S. Imberti, R. M. Madero-Castro, S. Calero, C. O. Ania, R. J. Jiménez-Riobóo, M. C. Gutiérrez, M. L. Ferrer and F. del Monte, *ACS Sustainable Chem. Eng.*, 2020, **8**, 12120–12131.
72 M. J. Roldán-Ruiz, R. J. Jiménez-Riobóo, M. C. Gutiérrez, M. L. Ferrer and F. del Monte, *J. Mol. Liq.*, 2019, **284**, 175–181.
73 H. Zhang, X. Lu, L. González-Aguilera, M. L. Ferrer, F. D. Monte and M. C. Gutiérrez, *J. Chem. Phys.*, 2021, **154**, 184501.
74 V. Agieienko and R. Buchner, *J. Chem. Eng. Data*, 2020, **65**, 1900–1910.
75 B. Soares, D. J. P. Tavares, J. L. Amaral, A. J. D. Silvestre, C. S. R. Freire and J. A. P. Coutinho, *ACS Sustainable Chem. Eng.*, 2017, **5**, 4056–4065.
76 B. Soares, A. J. D. Silvestre, P. C. Rodrigues Pinto, C. S. R. Freire and J. A. P. Coutinho, *ACS Sustainable Chem. Eng.*, 2019, **7**, 12485–12493.
77 E. Maia and S. Perez, *Acta Crystallogr., Sect. B: Struct. Crystallogr. Cryst. Chem.*, 1982, **38**, 849–852.

78 H. Chanzy, S. Nawrot, A. Peguy, P. Smith and J. Chevalier, *J. Polym. Sci., Polym. Phys. Ed.*, 1982, **20**, 1909–1924.
79 B. D. Rabideau and A. E. Ismail, *Phys. Chem. Chem. Phys.*, 2015, **17**, 5767–5775.
80 H. Zhang, L. González-Aguilera, D. López, M. Luisa Ferrer, F. del Monte and M. C. Gutiérrez, *J. Mol. Liq.*, 2022, **358**, 119113.
81 W.-J. Chen, C.-X. Zhao, B.-Q. Li, T.-Q. Yuan and Q. Zhang, *Green Chem.*, 2022, **24**, 565–584.
82 X. Wu, J. Jiang, C. Wang, J. Liu, Y. Pu, A. Ragauskas, S. Li and B. Yang, *Biofuels, Bioprod. Biorefin.*, 2020, **14**, 650–672.
83 J. Zhu, C. Yan, X. Zhang, C. Yang, M. Jiang and X. Zhang, *Prog. Energy Combust. Sci.*, 2020, **76**, 100788.
84 N. A. Banek, D. T. Abele, K. R. McKenzie and M. J. Wagner, *ACS Sustainable Chem. Eng.*, 2018, **6**, 13199–13207.
85 W. Zhang, J. Yin, Z. Lin, H. Lin, H. Lu, Y. Wang and W. Huang, *Electrochim. Acta*, 2015, **176**, 1136–1142.
86 M. Culebras, H. Geaney, A. Beaucamp, P. Upadhyaya, E. Dalton, K. M. Ryan and M. N. Collins, *ChemSusChem*, 2019, **12**, 4516–4521.
87 X. Niu, J. Zhou, T. Qian, M. Wang and C. Yan, *Nanotechnology*, 2017, **28**, 405401–405401.
88 C.-Y. Chou, J.-R. Kuo and S.-C. Yen, *ACS Sustainable Chem. Eng.*, 2018, **6**, 4759–4766.
89 L. Du, W. Wu, C. Luo, H. Zhao, D. Xu, R. Wang and Y. Deng, *Solid State Ionics*, 2018, **319**, 77–82.
90 H. P. C. K. Chan, G. Liu, K. McIlwrath, X. F. Zhang, R. A. Huggins and Y. Cui, *Nat. Nanotechnol.*, 2008, **3**, 31–35.
91 I. S. Aminu, H. Geaney, S. Imtiaz, T. E. Adegoke, N. Kapuria, G. A. Collins and K. M. Ryan, *Adv. Funct. Mater.*, 2020, 2003278, DOI: **10.1002/adfm.202003278**.
92 Y. Fan, Q. Zhang, Q. Xiao, X. Wang and K. Huang, *Carbon*, 2013, **59**, 264–269.
93 S. Karuppiah, C. Keller, P. Kumar, P.-H. Jouneau, D. Aldakov, J.-B. Ducros, G. R. Lapertot, P. Chenevier and C. D. Haon, *ACS Nano*, 2020, **14**, 12006–12015.
94 T. Kennedy, E. Mullane, H. Geaney, M. Osiak, C. O'Dwyer and K. M. Ryan, *Nano Lett.*, 2014, **14**, 716–723.
95 S. Imtiaz, I. S. Amiinu, D. Storan, N. Kapuria, H. Geaney, T. Kennedy and K. M. Ryan, *Adv. Mater.*, 2021, e2105917, DOI: **10.1002/adma.202105917**.
96 Y. Xi, S. Huang, D. Yang, X. Qiu, H. Su, C. Yi and Q. Li, *Green Chem.*, 2020, **22**, 4321–4433.
97 P. K. Nayak, L. Yang, W. Brehm and P. Adelhelm, *Angew. Chem., Int. Ed.*, 2018, **57**, 102–120.
98 C. Delmas, *Adv. Energy Mater.*, 2018, **8**, 1703137.
99 W. Zhang, J. Yin, W. Wang, Z. Bayhan and H. N. Alshareef, *Nano Energy*, 2021, **83**, 105792.
100 K. Nobuhara, H. Nakayama, M. Nose, S. Nakanishi and H. Iba, *J. Power Sources*, 2013, **243**, 585–587.
101 B. Jache and P. Adelhelm, *Angew. Chem., Int. Ed.*, 2014, **53**, 10169–10173.
102 Q. Liu, R. Xu, D. Mu, G. Tan, H. Gao, N. Li, R. Chen and F. Wu, *Carbon Energy*, 2022, **4**(3), 458–479.
103 Z. L. Xu, G. Yoon, K. Y. Park, H. Park, O. Tamwattana, S. Joo Kim, W. M. Seong and K. Kang, *Nat. Commun.*, 2019, **10**, 2598.
104 I. Hasa, X. Dou, D. Buchholz, Y. Shao-Horn, J. Hassoun, S. Passerini and B. Scrosati, *J. Power Sources*, 2016, **310**, 26–31.
105 X.-R. Zhang, J.-Y. Yang, Z.-Y. Ren, K.-Y. Xie, Q. Ye, F. Xu and X.-R. Liu, *New Carbon Mater.*, 2022, **37**, 371–379.
106 D. A. Stevens and J. R. Dahn, *J. Electrochem. Soc.*, 2000, **147**, 1271.
107 B. Xiao, T. Rojo and X. Li, *ChemSusChem*, 2019, **12**, 133–144.
108 W.-J. Chen, C.-X. Zhao, B.-Q. Li, T.-Q. Yuan and Q. Zhang, *Green Chem.*, 2022, **24**, 565–584.
109 X. Dou, I. Hasa, D. Saurel, C. Vaalma, L. Wu, D. Buchholz, D. Bresser, S. Komaba and S. Passerini, *Mater. Today*, 2019, **23**, 87–104.
110 D. G. Kizzire, A. M. Richter, D. P. Harper and D. J. Keffer, *ACS Omega*, 2021, **6**, 19883–19892.
111 X. Dou, I. Hasa, M. Hekmatfar, T. Diemant, R. J. Behm, D. Buchholz and S. Passerini, *ChemSusChem*, 2017, **10**, 2668–2676.
112 X. Lin, Y. Liu, H. Tan and B. Zhang, *Carbon*, 2020, **157**, 316–323.
113 Y. Lu, C. Zhao, X. Qi, Y. Qi, H. Li, X. Huang, L. Chen and Y.-S. Hu, *Adv. Energy Mater.*, 2018, **8**(17), 1703012.
114 Z. Wei, H.-X. Zhao, Y.-B. Niu, S.-Y. Zhang, Y.-B. Wu, H.-J. Yan, S. Xin, Y.-X. Yin and Y.-G. Guo, *Mater. Chem. Front.*, 2021, **5**, 3911–3917.
115 C. M. Ghimbeu, B. Zhang, A. Martinez de Yuso, B. Réty and J.-M. Tarascon, *Carbon*, 2019, **153**, 634–647.
116 C. Marino, J. Cabanero, M. Povia and C. Villevieille, *J. Electrochem. Soc.*, 2018, **165**, A1400–A1408.
117 S. Alvin, D. Yoon, C. Chandra, H. S. Cahyadi, J.-H. Park, W. Chang, K. Y. Chung and J. Kim, *Carbon*, 2019, **145**, 67–81.
118 D. Yoon, J. Hwang, W. Chang and J. Kim, *ACS Appl. Mater. Interfaces*, 2018, **10**, 569–581.
119 R. F. Susanti, S. Alvin and J. Kim, *J. Ind. Eng. Chem.*, 2020, **91**, 317–329.
120 K. Peuvot, O. Hosseinaei, P. Tomani, D. Zenkert and G. Lindbergh, *J. Electrochem. Soc.*, 2019, **166**, A1984–A1990.
121 G. Shi, Z. Han, L. Hu, B. Wang and F. Huang, *ChemElectroChem*, 2022, **9**, 304–315.
122 L. Fan, Z. Shi, Q. Ren, L. Yan, F. Zhang and L. Fan, *Green Energy Environ.*, 2021, **6**, 220–228.
123 L. Fan, X. Zhang, L. Fan, L. Yan, Z. Wang, W. Lei, D. Ruan and Z. Shi, *ACS Appl. Energy Mater.*, 2021, **4**, 11436–11446.
124 Z. Li, C. Bommier, Z. S. Chong, Z. Jian, T. W. Surta, X. Wang, Z. Xing, J. C. Neuefeind, W. F. Stickle, M. Dolgos, P. A. Greaney and X. Ji, *Adv. Energy Mater.*, 2017, **7**, 1602894.
125 S. Chen, F. Feng and Z.-F. Ma, *Compos. Commun.*, 2020, **22**, 106890.
126 X. Yuan, B. Zhu, J. Feng, C. Wang, X. Cai and R. Qin, *Chem. Eng. J.*, 2021, **405**, 126897.

127 Z. Wu, L. Wang, J. Huang, J. Zou, S. Chen, H. Cheng, C. Jiang, P. Gao and X. Niu, *Electrochim. Acta*, 2019, **306**, 446–453.
128 Z. Wu, J. Zou, S. Shabanian, K. Golovin and J. Liu, *Chem. Eng. J.*, 2022, **427**, 130972.
129 Z. Wu, J. Zou, Y. Zhang, X. Lin, D. Fry, L. Wang and J. Liu, *Chem. Eng. J.*, 2022, **427**, 131547.
130 L. Tao, L. Liu, R. Chang, H. He, P. Zhao and J. Liu, *J. Power Sources*, 2020, **463**, 228172.
131 K. Jiang, X. Tan, S. Zhai, K. Cadien and Z. Li, *Nano Res.*, 2021, **14**, 4664–4673.
132 M. Liu, D. Jing, Y. Shi and Q. Zhuang, *J. Mater. Sci.: Mater. Electron.*, 2019, **30**, 8911–8919.
133 J. Xu, C. Fan, M. Ou, S. Sun, Y. Xu, Y. Liu, X. Wang, Q. Li, C. Fang and J. Han, *Chem. Mater.*, 2022, **34**, 4202–4211.
134 C. del Mar Saavedra Rios, L. Simonin, C. M. Ghimbeu, C. Vaulot, D. da Silva Perez and C. Dupont, *Fuel Process. Technol.*, 2022, **231**, 107223.
135 J. L. Espinoza-Acosta, P. I. Torres-Chávez, J. L. Olmedo-Martínez, A. Vega-Rios, S. Flores-Gallardo and E. A. Zaragoza-Contreras, *J. Energy Chem.*, 2018, **27**, 1422–1438.
136 J. Wang, H. Yin, Z. Wang, J. Gao, Q. Jiang, Y. Xu and Z. Chen, *Asia–Pac. J. Chem. Eng.*, 2022, **17**, e2768.
137 H. Zhang, W. Zhang and F. Huang, *ACS Appl. Mater. Interfaces*, 2021, **13**, 61180–61188.
138 H. Zhang, W. Zhang, H. Ming, J. Pang, H. Zhang, G. Cao and Y. Yang, *Chem. Eng. J.*, 2018, **341**, 280–288.
139 C. Li, Y. Sun, Q. Wu, X. Liang, C. Chen and H. Xiang, *Chem. Commun.*, 2020, **56**, 6078–6081.
140 E. Stojanovska, E. S. Pampal, A. Kilic, M. Quddus and Z. Candan, *Composites, Part B*, 2019, **158**, 239–248.
141 J. Zhang, B. Yu, Y. Zhang and C. Wang, *Energy Technol.*, 2020, **8**(3), 1901423.
142 Y. Li, Y.-S. Hu, H. Li, L. Chen and X. Huang, *J. Mater. Chem. A*, 2016, **4**, 96–104.
143 Y. Zhang, Y. Zhu, J. Zhang, S. Sun, C. Wang, M. Chen and J. Zeng, *Energy Technol.*, 2019, **8**(1), 1900694.
144 J. Jin, B.-J. Yu, Z.-Q. Shi, C.-Y. Wang and C.-B. Chong, *J. Power Sources*, 2014, **272**, 800–807.
145 J. Zhang, J. Duan, Y. Zhang, M. Chen, K. Ji and C. Wang, *ChemElectroChem*, 2021, **8**, 3544–3552.
146 L. Du, W. Wu, C. Luo, D. Xu, H. Guo, R. Wang, T. Zhang, J. Wang and Y. Deng, *J. Electrochem. Soc.*, 2019, **166**, A423–A428.
147 M. Chen, F. Luo, Y. Liao, C. Liu, D. Xu, Z. Wang, Q. Liu, D. Wang, Y. Ye, S. Li, D. Wang and Z. Zheng, *J. Electroanal. Chem.*, 2022, **919**, 116526.
148 M. Ue, K. Sakaushi and K. Uosaki, *Mater. Horiz.*, 2020, **7**, 1937–1954.
149 A. Manthiram, Y. Fu, S.-H. Chung, C. Zu and Y.-S. Su, *Chem. Rev.*, 2014, **114**, 11751–11787.
150 J. B. Robinson, K. Xi, R. V. Kumar, A. C. Ferrari, H. Au, M.-M. Titirici, A. Parra-Puerto, A. Kucernak, S. D. S. Fitch, N. Garcia-Araez, Z. L. Brown, M. Pasta, L. Furness, A. J. Kibler, D. A. Walsh, L. R. Johnson, C. Holc, G. N. Newton, N. R. Champness, F. Markoulidis, C. Crean, R. C. T. Slade, E. I. Andritsos, Q. Cai, S. Babar, T. Zhang, C. Lekakou, N. Kulkarni, A. J. E. Rettie, R. Jervis, M. Cornish, M. Marinescu, G. Offer, Z. Li, L. Bird, C. P. Grey, M. Chhowalla, D. D. Lecce, R. E. Owen, T. S. Miller, D. J. L. Brett, S. Liatard, D. Ainsworth and P. R. Shearing, *J. Phys.: Energy*, 2021, **3**, 031501.
151 A. Manthiram, Y. Fu and Y.-S. Su, *Acc. Chem. Res.*, 2013, **46**, 1125–1134.
152 H. J. Peng, J. Q. Huang, X. B. Cheng and Q. Zhang, *Adv. Energy Mater.*, 2017, **7**, 1700260.
153 D. Su, D. Zhou, C. Wang and G. Wang, *Adv. Funct. Mater.*, 2018, **28**, 1870273.
154 F. Yu, Y. Li, M. Jia, T. Nan, H. Zhang, S. Zhao and Q. Shen, *J. Alloys Compd.*, 2017, **709**, 677–685.
155 Y. Liu, H. Guo, B. Zhang, G. Wen, R. Vajtai, L. Wu, P. M. Ajayan and L. Wang, *Batteries Supercaps*, 2020, **3**, 1201–1208.
156 W.-J. Kwak, D. S. Rosy, C. Xia, H. Kim, L. R. Johnson, P. G. Bruce, L. F. Nazar, Y.-K. Sun, A. A. Frimer, M. Noked, S. A. Freunberger and D. Aurbach, *Chem. Rev.*, 2020, **120**, 6626–6683.
157 J. Fu, R. Liang, G. Liu, A. Yu, Z. Bai, L. Yang and Z. Chen, *Adv. Mater.*, 2019, **31**, e1805230.
158 G. Zhang, Y. Yao, T. Zhao, M. Wang and R. Chen, *ACS Appl. Mater. Interfaces*, 2020, **12**, 16521.
159 A. Arul, H. Pak, K. U. Moon, M. Christy, M. Y. Oh and K. S. Nahm, *Appl. Catal., B*, 2018, **220**, 488–496.
160 P. Li, H. Wang, W. Fan, M. Huang, J. Shi, Z. Shi and S. Liu, *Chem. Eng. J.*, 2021, **421**, 129704.
161 D. Bresser, D. Buchholz, A. Moretti, A. Varzi and S. Passerini, *Energy Environ. Sci.*, 2018, **11**, 396–3127.
162 A. Cholewinski, P. Si, M. Uceda, M. Pope and B. Zhao, *Polymers*, 2021, **13**, 1–20.
163 T. Chen, J. Hu, L. Zhang, J. Pan, Y. Liu and Y.-T. Cheng, *J. Power Sources*, 2017, **362**, 236–242.
164 C. Luo, L. Du, W. Wu, H. Xu, G. Zhang, S. Li, C. Wang, Z. Lu and Y. Deng, *ACS Sustainable Chem. Eng.*, 2018, **6**, 12621–12629.
165 Y. Ma, K. Chen, J. Ma, G. Xu, S. Dong, B. Chen, J. Li, Z. Chen, X. Zhou and G. Cui, *Energy Environ. Sci.*, 2019, **12**, 273–280.
166 S. Wang, L. Zhang, A. Wang, X. Liu, J. Chen, Z. Wang, Q. Zeng, H.-H. Zhou, X. Jiang and L. Zhang, *ACS Sustainable Chem. Eng.*, 2018, **6**, 14460–14469.
167 H. Liu, L. Mulderrig, D. Hallinan and H. Chung, *Macromol. Rapid Commun.*, 2021, **42**, e2000428.
168 P. Arora and Z. Zhang, *Chem. Rev.*, 2004, **104**, 4419–4462.
169 W. Luo, S. Cheng, M. Wu, X. Zhang, D. Yang and X. Rui, *J. Power Sources*, 2021, **509**, 230372.
170 M. Zhao, J. Wang, C. Chong, X. Yu, L. Wang and Z. Shi, *RSC Adv.*, 2015, **5**, 11115–11112.
171 M. O. Bamgbopa, A. Fetyan, M. Vagin and A. A. Adelodun, *J. Energy Storage*, 2022, **50**, 104352.
172 M. C. Ribadeneyra, L. Grogan, H. Au, P. Schlee, S. Herou, T. Neville, P. L. Cullen, M. D. R. Kok, O. Hosseinaei,

S. Danielsson, P. Tomani, M. M. Titirici, D. J. L. Brett, P. R. Shearing, R. Jervis and A. B. Jorge, *Carbon*, 2020, **157**, 847–856.
173 J. Ye, Y. Cheng, L. Sun, M. Ding, C. Wu, D. Yuan, X. Zhao, C. Xiang and C. Jia, *J. Membr. Sci.*, 2019, **572**, 110–118.
174 J. Ye, D. Yuan, M. Ding, Y. Long, T. Long, L. Sun and C. Jia, *J. Power Sources*, 2021, **482**, 229023.
175 A. Mukhopadhyay, J. Hamel, R. Katahira and H. Zhu, *ACS Sustainable Chem. Eng.*, 2018, **6**, 5394–5400.
176 C. Schütter, S. Pohlmann and A. Balducci, *Adv. Energy Mater.*, 2019, **9**, 1900334.
177 P. Schlee, S. Herou, R. Jervis, P. R. Shearing, D. J. L. Brett, D. Baker, O. Hosseinaei, P. Tomani, M. M. Murshed, Y. Li, M. J. Mostazo-Lopez, D. Cazorla-Amoros, A. B. Jorge Sobrido and M. M. Titirici, *Chem. Sci.*, 2019, **10**, 2980–2988.
178 P. Schlee, O. Hosseinaei, D. Baker, A. Landmér, P. Tomani, M. J. Mostazo-López, D. Cazorla-Amorós, S. Herou and M.-M. Titirici, *Carbon*, 2019, **145**, 470–480.
179 S. Herou, M. C. Ribadeneyra, R. Madhu, V. Araullo-Peters, A. Jensen, P. Schlee and M. Titirici, *Green Chem.*, 2019, **21**, 550–559.
180 Z. Peng, Y. Zou, S. Xu, W. Zhong and W. Yang, *ACS Appl. Mater. Interfaces*, 2018, **10**, 22190–22200.
181 J. Xu, X. Zhou, M. Chen, S. Shi and Y. Cao, *Microporous Mesoporous Mater.*, 2018, **265**, 258–265.
182 F. N. Ajjan, N. Casado, T. Rębiś, A. Elfwing, N. Solin, D. Mecerreyes and O. Inganäs, *J. Mater. Chem. A*, 2016, **4**, 1838–1847.
183 E. Raymundo-Piñero, F. Leroux and F. Béguin, *Adv. Mater.*, 2006, **18**, 1877–1882.
184 P. J. Suhas Carrott and M. M. Ribeiro Carrott, *Bioresour. Technol.*, 2007, **98**, 2301–2312.
185 F. Jianhui, Y. Boyuan, N. HaoXiong, H. Xiaojun and W. Ting, *2011 International Conference on Materials for Renewable Energy & Environment*, 2011, DOI: **10.1109/ICMREE.2011.5930944**.
186 B. Du, H. Zhu, L. Chai, J. Cheng, X. Wang, X. Chen, J. Zhou and R.-C. Sun, *Ind. Crops Prod.*, 2021, **170**, 113745.
187 B. Yu, Z. Chang and C. Wang, *Mater. Chem. Phys.*, 2016, **181**, 187–193.
188 L. Wang, L. Xie, X. Feng, H. Ma, X. Li and J. Zhou, *ACS Omega*, 2021, **6**, 33171–33179.
189 N. Guo, M. Li, X. Sun, F. Wang and R. Yang, *Green Chem.*, 2017, **19**, 2595–2602.
190 A. M. Navarro-Suárez, J. Carretero-González, V. Roddatis, E. Goikolea, J. Ségalini, E. Redondo, T. Rojo and R. Mysyk, *RSC Adv.*, 2014, **4**, 48336–48343.
191 W. Zhang, M. Zhao, R. Liu, X. Wang and H. Lin, *Colloids Surf., A*, 2015, **484**, 518–527.
192 K. Wang, Y. Cao, X. Wang, M. A. Castro, B. Luo, Z. Gu, J. Liu, J. D. Hoefelmeyer and Q. Fan, *J. Power Sources*, 2016, **307**, 462–467.
193 K. Wang, M. Xu, Y. Gu, Z. Gu and Q. H. Fan, *J. Power Sources*, 2016, **332**, 180–186.
194 M. Klose, R. Reinhold, F. Logsch, F. Wolke, J. Linnemann, U. Stoeck, S. Oswald, M. Uhlemann, J. Balach, J. Markowski, P. Ay and L. Giebeler, *ACS Sustainable Chem. Eng.*, 2017, **5**, 4094–4102.
195 Z.-Z. Chang, B.-J. Yu and C.-Y. Wang, *J. Solid State Electrochem.*, 2016, **20**, 1405–1412.
196 S. Hu and Y.-L. Hsieh, *RSC Adv.*, 2017, **7**, 30459–30468.
197 H. C. Ho, N. A. Nguyen, K. M. Meek, D. M. Alonso, S. H. Hakim and A. K. Naskar, *ChemSusChem*, 2018, **11**, 2953–2959.
198 W. Li, Y. Zhang, L. Das, Y. Wang, M. Li, N. Wanninayake, Y. Pu, D. Y. Kim, Y.-T. Cheng, A. J. Ragauskas and J. Shi, *RSC Adv.*, 2018, **8**, 38721–38732.
199 X. Zhang, W. Jian, L. Zhao, F. Wen, J. Chen, J. Yin, Y. Qin, K. Lu, W. Zhang and X. Qiu, *Colloids Surf., A*, 2022, **636**, 128191.
200 Z. Zhao, S. Hao, P. Hao, Y. Sang, A. Manivannan, N. Wu and H. Liu, *J. Mater. Chem. A*, 2015, **3**, 15049–15056.
201 L. Wang, J. Wu, H. Ma, G. Han, D. Yang, Y. Chen and J. Zhou, *Energy Fuels*, 2021, **35**, 8303–8312.
202 E. Gonzalez-Serrano, T. Cordero, J. Rodríguez-Mirasol and J. J. Rodríguez, *Ind. Eng. Chem. Res.*, 1997, **36**, 4832–4838.
203 Y. Song, J. Liu, K. Sun and W. Xu, *RSC Adv.*, 2017, **7**, 48324–48332.
204 C. Ma, L. Wu, M. Dirican, H. Cheng, J. Li, Y. Song, J. Shi and X. Zhang, *J. Colloid Interface Sci.*, 2021, **586**, 412–422.
205 C. M. Fierro, J. Górka, J. A. Zazo, J. J. Rodriguez, J. Ludwinowicz and M. Jaroniec, *Carbon*, 2013, **62**, 233–239.
206 Y. Xi, X. Liu, W. Xiong, H. Wang, X. Ji, F. Kong, G. Yang and J. Xu, *Ind. Crops Prod.*, 2021, **174**, 114184.
207 M. J. Valero-Romero, E. M. Márquez-Franco, J. Bedia, J. Rodríguez-Mirasol and T. Cordero, *Microporous Mesoporous Mater.*, 2014, **196**, 68–78.
208 D. Salinas-Torres, R. Ruiz-Rosas, M. J. Valero-Romero, J. Rodríguez-Mirasol, T. Cordero, E. Morallón and D. Cazorla-Amorós, *J. Power Sources*, 2016, **326**, 641–651.
209 J. Tian, Z. Liu, Z. Li, W. Wang and H. Zhang, *RSC Adv.*, 2017, **7**, 12089–12097.
210 P. L. Kool, M. D. Ortiz and C. A. van Gestel, *Environ. Pollut.*, 2011, **159**, 2713–2719.
211 N. M. Franklin, N. J. Rogers, S. C. Apte, G. E. Batley, G. E. Gadd and P. S. Casey, *Environ. Sci. Technol.*, 2007, **41**, 8484–8490.
212 A. Perez-Lopez, G. Nunez-Nogueira, C. A. Alvarez-Gonzalez, S. De la Rosa-Garcia, M. Uribe-Lopez, P. Quintana and E. S. Pena-Marin, *Environ. Sci. Pollut. Res. Int.*, 2020, **27**, 22441–22450.
213 G. Sima, L. Gan, L. Chang, Y. Cui and R. K. Kankala, *Microporous Mesoporous Mater.*, 2021, **323**, 111192.
214 D. Saha, Y. Li, Z. Bi, J. Chen, J. K. Keum, D. K. Hensley, H. A. Grappe, H. M. Meyer 3rd, S. Dai, M. P. Paranthaman and A. K. Naskar, *Langmuir*, 2014, **30**, 900–910.
215 W. Zhang, H. Lin, Z. Lin, J. Yin, H. Lu, D. Liu and M. Zhao, *ChemSusChem*, 2015, **8**, 2114–2122.
216 D. Liu, W. Zhang, D. Liu, J. Yang, J. Yin and H. Lin, *J. Mater. Sci.: Mater. Electron.*, 2021, **32**, 7009–7018.
217 J. H. Park, H. H. Rana, J. Y. Lee and H. S. Park, *J. Mater. Chem. A*, 2019, **7**, 16962–16968.

218 E. Svinterikos, I. Zuburtikudis and M. Al-Marzouqi, *ACS Sustainable Chem. Eng.*, 2020, **8**, 13868–13893.
219 C. Ma, Z. Li, J. Li, Q. Fan, L. Wu, J. Shi and Y. Song, *Appl. Surf. Sci.*, 2018, **456**, 568–576.
220 X. Wang, W. Zhang, M. Chen and X. Zhou, *Polymers*, 2018, **10**, 1306.
221 Q. Cao, Y. Zhang, J. Chen, M. Zhu, C. Yang, H. Guo, Y. Song, Y. Li and J. Zhou, *Ind. Crops Prod.*, 2020, **148**, 112181.
222 A. Bachs-Herrera, O. Yousefzade, L. J. del Valle and J. Puiggali, *Appl. Sci.*, 2021, **11**, 1808.
223 Y. Aranishi and Y. Nishio, in *Blends and Graft Copolymers of Cellulosics: Toward the Design and Development of Advanced Films and Fibers*, ed. Y. Nishio, Y. Teramoto, R. Kusumi, K. Sugimura and Y. Aranishi, Springer International Publishing, Cham, 2017, pp. 109–125, DOI: 10.1007/978-3-319-55321-4_5.
224 S. P. Maradur, C. H. Kim, S. Y. Kim, B.-H. Kim, W. C. Kim and K. S. Yang, *Synth. Met.*, 2012, **162**, 453–459.
225 X.-Y. Wang, G.-Y. Feng, M.-J. Li and M.-Q. Ge, *Polym. Bull.*, 2019, **76**, 2097–2111.
226 C. Lu, C. Blackwell, Q. Ren and E. Ford, *ACS Sustainable Chem. Eng.*, 2017, **5**, 2949–2959.
227 M. Yanilmaz and X. Zhang, *Polymers*, 2015, **7**, 629–643.
228 W. Qu, J. Yang, X. Sun, X. Bai, H. Jin and M. Zhang, *Int. J. Biol. Macromol.*, 2021, **189**, 768–784.
229 P. Schlee, O. Hosseinaei, C. A. O' Keefe, M. J. Mostazo-López, D. Cazorla-Amorós, S. Herou, P. Tomani, C. P. Grey and M.-M. Titirici, *J. Mater. Chem. A*, 2020, **8**, 23543–23554.
230 I. Khan, B. Hararak and G. F. Fernando, *Sci. Rep.*, 2021, **11**, 16237.
231 X. Xu, J. Zhou, L. Jiang, G. Lubineau, S. A. Payne and D. Gutschmidt, *Carbon*, 2014, **80**, 91–102.
232 W. J. Youe, S. J. Kim, S. M. Lee, S. J. Chun, J. Kang and Y. S. Kim, *Int. J. Biol. Macromol.*, 2018, **112**, 943–950.
233 D. Lei, X.-D. Li, M.-K. Seo, M.-S. Khil, H.-Y. Kim and B.-S. Kim, *Polymer*, 2017, **132**, 31–40.
234 S. Hu, S. Zhang, N. Pan and Y.-L. Hsieh, *J. Power Sources*, 2014, **270**, 106–112.
235 W. Fang, S. Yang, T.-Q. Yuan, A. Charlton and R.-C. Sun, *Ind. Eng. Chem. Res.*, 2017, **56**, 9551–9559.
236 X. Ma, P. Kolla, Y. Zhao, A. L. Smirnova and H. Fong, *J. Power Sources*, 2016, **325**, 541–548.
237 C. Lai, Z. Zhou, L. Zhang, X. Wang, Q. Zhou, Y. Zhao, Y. Wang, X.-F. Wu, Z. Zhu and H. Fong, *J. Power Sources*, 2014, **247**, 134–141.
238 H. Khayyam, R. N. Jazar, S. Nunna, G. Golkarnarenji, K. Badii, S. M. Fakhrhoseini, S. Kumar and M. Naebe, *Prog. Mater. Sci.*, 2020, **107**, 100575.
239 Z. Xiong, N. Chen and Q. Wang, *J. Appl. Polym. Sci.*, 2020, **137**, 49385.
240 J. Yang, Y. Wang, J. Luo and L. Chen, *ACS Omega*, 2018, **3**, 4647–4656.
241 F. Fu, D. Yang, W. Zhang, H. Wang and X. Qiu, *Chem. Eng. J.*, 2020, **392**, 123721.
242 H. Li, F. Shi, Q. An, S. Zhai, K. Wang and Y. Tong, *Int. J. Biol. Macromol.*, 2021, **166**, 923–933.
243 F. Liu, Z. Wang, H. Zhang, L. Jin, X. Chu, B. Gu, H. Huang and W. Yang, *Carbon*, 2019, **149**, 105–116.
244 W.-M. Yin, L.-F. Tian, B. Pang, Y.-R. Guo, S.-J. Li and Q.-J. Pan, *Int. J. Biol. Macromol.*, 2020, **156**, 988–996.
245 F. Shi, J. Li, J. Xiao, X. Zhao, H. Li, Q. An, S. Zhai, K. Wang, L. Wei and Y. Tong, *Int. J. Biol. Macromol.*, 2021, **190**, 11–18.
246 M. Zhou, A. Bahi, Y. Zhao, L. Lin, F. Ko, P. Servati, S. Soltanian, P. Wang, Y. Yu, Q. Wang and Z. Cai, *Chem. Eng. J.*, 2021, **409**, 128214.
247 T. Wang, S. Hu, D. Wu, W. Zhao, W. Yu, M. Wang, J. Xu and J. Zhang, *J. Mater. Chem. A*, 2021, **9**, 11839–11852.
248 M. Yuan, F. Luo, Y. Rao, Y. Wang, J. Yu, H. Li and X. Chen, *J. Power Sources*, 2021, **513**, 230558.
249 Z. Dai, P.-G. Ren, W. He, X. Hou, F. Ren, Q. Zhang and Y.-L. Jin, *Renewable Energy*, 2020, **162**, 613–623.
250 B. Du, X. Wang, L. Chai, X. Wang, Z. Pan, X. Chen, J. Zhou and R.-C. Sun, *Int. J. Biol. Macromol.*, 2022, **194**, 632–643.
251 Z.-R. Hu, D.-D. Li, T.-H. Kim, M.-S. Kim, T. Xu, M.-G. Ma, S.-E. Choi and C. Si, *Front. Chem.*, 2022, **10**, 841956.
252 M. Culebras, C. M. Gómez and A. Cantarero, *J. Mater. Chem. A*, 2014, **2**, 10109.
253 M. Culebras, C. Gómez and A. Cantarero, *Materials*, 2014, **7**, 6701–6732.
254 M. Culebras, B. Uriol, C. M. Gomez and A. Cantarero, *Phys. Chem. Chem. Phys.*, 2015, **17**, 15140–15145.
255 M. Culebras, M. M. de Lima, C. Gómez and A. Cantarero, *J. Appl. Polym. Sci.*, 2017, **134**(3), 43927.
256 J. Gao, C. Liu, L. Miao, X. Wang, C. Li, R. Huang, Y. Chen and S. Tanemura, *Synth. Met.*, 2015, **210**, 342–351.
257 H. Shi, C. Liu, J. Xu, H. Song, B. Lu, F. Jiang, W. Zhou, G. Zhang and Q. Jiang, *ACS Appl. Mater. Interfaces*, 2013, **5**, 12811–12819.
258 M. Culebras, A. M. Igual-Muñoz, C. Rodríguez-Fernández, M. I. Gómez-Gómez, C. Gomez and A. Cantarero, *ACS Appl. Mater. Interfaces*, 2017, **9**, 20826–20832.
259 N. Dalton, R. P. Lynch, M. N. Collins and M. Culebras, *Int. J. Biol. Macromol.*, 2019, **121**, 472–479.
260 M. Culebras, G. Ren, S. O'Connell, J. J. Vilatela and M. N. Collins, *Adv. Sustainable Syst.*, 2020, **4**, 2000147.
261 X. Zhao, C. Huang, D. Xiao, P. Wang, X. Luo, W. Liu, S. Liu, J. Li, S. Li and Z. Chen, *ACS Appl. Mater. Interfaces*, 2021, **13**, 7600–7607.
262 J. Chen, J. Qi, J. He, Y. Yan, F. Jiang, Z. Wang and Y. Zhang, *ACS Appl. Mater. Interfaces*, 2022, **14**, 12748–12757.
263 R. Shu, R. Li, B. Lin, C. Wang, Z. Cheng and Y. Chen, *Biomass Bioenergy*, 2020, **132**, 105432.
264 P. Azadi, O. R. Inderwildi, R. Farnood and D. A. King, *Renewable Sustainable Energy Rev.*, 2013, **21**, 506–523.
265 H. Wang, L. Zhang, T. Deng, H. Ruan, X. Hou, J. R. Cort and B. Yang, *Green Chem.*, 2016, **18**, 2802–2810.
266 H. Wang, H. Wang, E. Kuhn, M. P. Tucker and B. Yang, *ChemSusChem*, 2018, **11**, 285–291.

267 M. M. Ambursa, J. C. Juan, Y. Yahaya, Y. H. Taufiq-Yap, Y.-C. Lin and H. V. Lee, *Renewable Sustainable Energy Rev.*, 2021, **138**, 110667.
268 M. Zhao, J. Hu, P. Lu, S. Wu, C. Liu and Y. Sun, *Fuel*, 2022, **326**, 125020.
269 C. G. Yoo, A. Dumitrache, W. Muchero, J. Natzke, H. Akinosho, M. Li, R. W. Sykes, S. D. Brown, B. Davison, G. A. Tuskan, Y. Pu and A. J. Ragauskas, *ACS Sustainable Chem. Eng.*, 2018, **6**, 2162–2168.
270 H. J. Pegoretti, L. de Souza, F. Muñoz, R. T. Mendonça, K. Sáez, R. Olave, C. Segura, D. P. L. de Souza, T. de Paula Protásio and R. Rodríguez-Soalleiro, *Renewable Energy*, 2021, **163**, 1802–1816.
271 H. Ohta, K. Yamamoto, M. Hayashi, G. Hamasaka, Y. Uozumi and Y. Watanabe, *Chem. Commun.*, 2015, **51**, 17000–17003.
272 H. Wang, H. Ruan, M. Feng, Y. Qin, H. Job, L. Luo, C. Wang, M. H. Engelhard, E. Kuhn, X. Chen, M. P. Tucker and B. Yang, *ChemSusChem*, 2017, **10**, 1846–1856.
273 T. Guo, Q. Xia, Y. Shao, X. Liu and Y. Wang, *Appl. Catal., A*, 2017, **547**, 30–36.
274 Y. Cao, S. S. Chen, S. Zhang, Y. S. Ok, B. M. Matsagar, K. C. W. Wu and D. C. W. Tsang, *Bioresour. Technol.*, 2019, **291**, 121878.
275 S. G. Yao, Ph.D., University of Kentucky, 2018.
276 S. G. Yao, J. K. Mobley, J. Ralph, M. Crocker, S. Parkin, J. P. Selegue and M. S. Meier, *ACS Sustainable Chem. Eng.*, 2018, **6**, 5990–5998.
277 S. Dabral, H. Wotruba, J. G. Hernández and C. Bolm, *ACS Sustainable Chem. Eng.*, 2018, **6**, 3242–3254.
278 Y. Wang, J. He and Y. Zhang, *CCS Chem.*, 2020, **2**, 107–117.
279 Y. Kang, X. Lu, G. Zhang, X. Yao, J. Xin, S. Yang, Y. Yang, J. Xu, M. Feng and S. Zhang, *ChemSusChem*, 2019, **12**, 4005–4013.
280 H. Chen, K. Wan, F. Zheng, Z. Zhang, Y. Zhang and D. Long, *Renewable Sustainable Energy Rev.*, 2021, **147**, 111217.
281 Z. Hao, S. Li, J. Sun, S. Li and F. Zhang, *Appl. Catal., B*, 2018, **237**, 366–372.
282 S. Li, Z. Hao, K. Wang, M. Tong, Y. Yang, H. Jiang, Y. Xiao and F. Zhang, *Chem. Commun.*, 2020, **56**, 11243–11246.
283 X. Wu, X. Fan, S. Xie, J. Lin, J. Cheng, Q. Zhang, L. Chen and Y. Wang, *Nat. Catal.*, 2018, **1**, 772–780.
284 Z. Xiang, W. Han, J. Deng, W. Zhu, Y. Zhang and H. Wang, *ChemSusChem*, 2020, **13**, 4199–4213.
285 H. Yoo, M.-W. Lee, S. Lee, J. Lee, S. Cho, H. Lee, H. G. Cha and H. S. Kim, *ACS Catal.*, 2020, **10**, 8465–8475.
286 M. Garedew, F. Lin, B. Song, T. M. DeWinter, J. E. Jackson, C. M. Saffron, C. H. Lam and P. T. Anastas, *ChemSusChem*, 2020, **13**, 4214–4237.
287 S. V. Obydenkova, P. D. Kouris, E. J. M. Hensen, H. J. Heeres and M. D. Boot, *Bioresour. Technol.*, 2017, **243**, 589–599.
288 I. O. f. Standardization, *Environmental management: life cycle assessment; requirements and guidelines*, ISO Geneva, Switzerland, 2006.
289 C. Culbertson, T. Treasure, R. Venditti, H. Jameel and R. Gonzalez, *Nord. Pulp Pap. Res. J.*, 2016, **31**, 30–40.
290 D. G. Kulas, M. C. Thies and D. R. Shonnard, *ACS Sustainable Chem. Eng.*, 2021, **9**, 5388–5395.
291 S. Zargar, J. G. Jiang, F. Jiang and Q. S. Tu, *Biofuels, Bioprod. Biorefin.*, 2022, **16**, 68–80.
292 D. Koch, M. Paul, S. Beisl, A. Friedl and B. Mihalyi, *J. Cleaner Prod.*, 2020, **245**, 118760.
293 L. Zeilerbauer, J. Lindorfer, R. Suss and B. Kamm, *Biofuels, Bioprod. Biorefin.*, 2022, **16**, 370–388.
294 P. N. Shinde, S. A. Mandavgane and V. Karadbhajane, *Environ. Sci. Pollut. Res.*, 2020, **27**, 25785–25793.
295 K. C. Teh, C. Y. Tan and I. M. L. Chew, *J. Environ. Chem. Eng.*, 2021, **9**, 105381.
296 F. Liu, X. Y. Dong, X. B. Zhao and L. Wang, *Energy Convers. Manage.*, 2021, **246**, 114653.
297 A. W. Bartling, M. L. Stone, R. J. Hanes, A. Bhatt, Y. M. Zhang, M. J. Biddy, R. Davis, J. S. Kruger, N. E. Thornburg, J. S. Luterbacher, R. Rinaldi, J. S. M. Samec, B. F. Sels, Y. Roman-Leshkov and G. T. Beckham, *Energy Environ. Sci.*, 2021, **14**, 4147–4168.
298 N. M. Kosamia, M. Samavi, K. Piok and S. K. Rakshit, *Fuel*, 2022, **324**, 124532.
299 E. Bernier, C. Lavigne and P. Y. Robidoux, *Int. J. Life Cycle Assess.*, 2013, **18**, 520–528.
300 C. Moretti, R. Hoefnagels, M. van Veen, B. Corona, S. Obydenkova, S. Russell, A. Jongerius, I. Vural-Gürsel and M. Junginger, *J. Cleaner Prod.*, 2022, **343**, 131063.
301 C. Moretti, B. Corona, R. Hoefnagels, M. van Veen, I. Vural-Gursel, T. Strating, R. Gosselink and M. Junginger, *Sci. Total Environ.*, 2022, **806**, 150316.
302 O. O. Tokede, A. Whittaker, R. Mankaa and M. Traverso, *Structures*, 2020, **25**, 190–199.
303 Y. C. Yue, M. Abdelsalam, A. Khater and M. Ghazy, *Constr. Build. Mater.*, 2022, **323**, 126608.
304 A. Khater, D. Luo, M. Abdelsalam, M. Ghazy and Jianxun, *Materials*, 2021, **14**, 6589.
305 J. E. McDevitt and W. J. Grigsby, *J. Polym. Environ.*, 2014, **22**, 537–544.
306 L. O. Cortat, N. C. Zanini, R. F. S. Barbosa, A. G. de Souza, D. S. Rosa and D. R. Mulinari, *J. Polym. Environ.*, 2021, **29**, 3210–3226.
307 M. L. Yang and K. A. Rosentrater, *Environ. Processes*, 2020, **7**, 553–561.
308 J. Hildebrandt, M. Budzinski, R. Nitzsche, A. Webe, A. Krombholz, D. Thran and A. Bezama, *Resour., Conserv. Recycl.*, 2019, **141**, 455–464.
309 C. Isola, H. L. Sieverding, A. Numan-Al-Mobin, R. Rajappagowda, E. A. Boakye, D. E. Raynie, A. L. Smirnova and J. J. Stone, *Int. J. Life Cycle Assess.*, 2018, **23**, 1761–1772.
310 M. Montazeri and M. J. Eckelman, *ACS Sustainable Chem. Eng.*, 2016, **4**, 708–718.
311 A. Corona, M. J. Biddy, D. R. Vardon, M. Birkved, M. Z. Hauschild and G. T. Beckham, *Green Chem.*, 2018, **20**, 3857–3866.

312 R. Akmalina and M. G. Pawitra, *Asia–Pac. J. Chem. Eng.*, 2020, **15**, e2436.
313 E. Budsberg, R. Morales-Vera, J. T. Crawford, R. Bura and R. Gustafson, *Biotechnol. Biofuels*, 2020, **13**, 154.
314 S. V. Mankar, M. N. G. Gonzalez, N. Warlin, N. G. Valsange, N. Rehnberg, S. Lundmark, P. Jannasch and B. Z. Zhang, *ACS Sustainable Chem. Eng.*, 2019, **7**, 19090–19103.
315 F. Hermansson, M. Janssen and M. Svanström, *J. Cleaner Prod.*, 2019, **223**, 946–956.
316 M. Secchi, V. Castellani, M. Orlandi and E. Collina, *BioResources*, 2019, **14**, 4832–4865.
317 S. Soam, M. Kapoor, R. Kumar, R. P. Gupta, S. K. Puri and S. S. V. Ramakumar, *J. Cleaner Prod.*, 2018, **197**, 732–741.
318 E. Budsberg, J. T. Crawford, H. Morgan, W. S. Chin, R. Bura and R. Gustafson, *Biotechnol. Biofuels*, 2016, **9**, 170.
319 J. K. Raman and E. Gnansounou, *Bioresour. Technol.*, 2015, **185**, 202–210.
320 A. W. Bartling, P. T. Benavides, S. D. Phillips, T. Hawkins, A. Singh, M. Wiatrowski, E. C. D. Tan, C. Kinchin, L. W. Ou, H. Cai, M. Biddy, L. Tao, A. Young, K. Brown, S. Y. Li, Y. H. Zhu, L. J. Snowden-Swan, C. R. Mevawala and D. J. Gaspar, *ACS Sustainable Chem. Eng.*, 2022, **10**(10), 6699–6712.
321 N. Mahendrasinh Kosamia, M. Samavi, K. Piok and S. Kumar Rakshit, *Fuel*, 2022, **324**, 124532.
322 T. Bicalho, J. Richard and C. Bessou, *Sustainability Account. Manage. Policy J.*, 2012, **3**, 218–234.
323 F. Hermansson, M. Janssen and M. Svanstrom, *Int. J. Life Cycle Assess.*, 2020, **25**, 1620–1632.
324 C. Moretti, B. Corona, R. Hoefnagels, I. Vural-Gursel, R. Gosselink and M. Junginger, *Sci. Total Environ.*, 2021, **806**(1), 150316.
325 K. Navare, W. Arts, G. Faraca, G. V. D. Bossche, B. Sels and K. V. Acker, *Resour., Conserv. Recycl.*, 2022, **186**, 106588.
326 J. Wenger, S. Pichler, A. Nayha and T. Stern, *Sustainability*, 2022, **14**, 2619.
327 G. Sandin, F. Royne, J. Berlin, G. M. Peters and M. Svanstrom, *J. Cleaner Prod.*, 2015, **93**, 213–221.
328 S. V. Obydenkova, P. D. Kouris, D. M. J. Smeulders, M. D. Boot and Y. van der Meer, *Biofuels, Bioprod. Biorefin.*, 2021, **15**, 1281–1300.
329 A. Arias, S. González-García, S. González-Rodríguez, G. Feijoo and M. T. Moreira, *Sci. Total Environ.*, 2020, **738**, 140357.
330 P. Yadav, D. Athanassiadis, I. Antonopoulou, U. Rova, P. Christakopoulos, M. Tysklind and L. Matsakas, *J. Cleaner Prod.*, 2021, **279**, 123515.
331 U. S. E. P. Agency, Overview for Renewable Fuel Standard, **https://www.epa.gov/renewable-fuel-standard-program/overview-renewable-fuel-standard**, (accessed 22/08/2022, 2022).